NASA CONTRACTOR REPORT

NASA CR-328

MEASUREMENTS OF NONEQUILIBRIUM EFFECTS IN AIR ON WEDGE-FLAT-PLATE AFTERBODY PRESSURES

by R. J. Vidal and F. Stoddard

Prepared under Contract No. NAS 1-2812 *by*
CORNELL AERONAUTICAL LABORATORY, INC.
Buffalo, N. Y.
for Langley Research Center

NATIONAL AERONAUTICS AND SPACE ADMINISTRATION • WASHINGTON, D. C. • NOVEMBER 1965

MEASUREMENTS OF NONEQUILIBRIUM EFFECTS IN AIR ON WEDGE-FLAT-PLATE AFTERBODY PRESSURES

By R. J. Vidal and F. Stoddard

Prepared under Contract No. NAS 1-2812 by
CORNELL AERONAUTICAL LABORATORY, INC.
Buffalo, N.Y.

for Langley Research Center

NATIONAL AERONAUTICS AND SPACE ADMINISTRATION

For sale by the Clearinghouse for Federal Scientific and Technical Information
Springfield, Virginia 22151 – Price $3.00

FOREWORD

This research was sponsored jointly by the Arnold Engineering and Development Center under Contract No. AF 49(600)-928, and by the National Aeronautics and Space Administration under Contract No. NAS 1-2812. The original experiments and analysis were supported by the AEDC, and subsequent clarifying experiments and data analysis were supported by NASA. The authors gratefully acknowledge the aid of Dr. J. Gordon Hall in suggesting the experiments and for the many stimulating discussions on the results.

ABSTRACT

Experimental heat transfer and pressure data are presented for a flat plate with large and small-scale wedge leading edges. These data, obtained in high temperature air, are compared with various theoretical estimates to determine the effects of thermochemical nonequilibrium. Data obtained with the small-scale model under high temperature conditions, in which the entire flowfield should be frozen, are found to correlate well with low temperature data if a non-linear temperature-viscosity relation is used in the similarity parameters. The data obtained under conditions in which the flowfield is not frozen show large nonequilibrium effects on after-body pressure; the pressure is 25%-35% less than the equilibrium-gas value. It is found that these effects can be estimated using nonequilibrium normal shock wave results to calculate the flow on the wedge face, and by assuming the flow is frozen in the expansion process at the wedge shoulder. At the low temperatures (3300°K) substantial effects result from vibrational nonequilibrium, while at the higher temperatures (6600°K) the effects result from vibrational and chemical nonequilibrium.

TABLE OF CONTENTS

LIST OF SYMBOLS

A	constant defined in Appendix A, Eq. (A-6)
C^*	$\dfrac{\mu(T^*)}{\mu(T_\infty)}\,\dfrac{T_\infty}{T^*}$
$C^{*'}$	$\dfrac{\mu(T^*)}{\mu(T_\infty)}\left(\dfrac{T_\infty}{T^*}\right)^\omega$
C_H	Stanton number, $\dfrac{q}{\rho_\infty U_\infty (H_o - H_w)}$
H_o	reservoir enthalpy
H_w	wall enthalpy
k	nose drag coefficient, $\dfrac{D_n}{1/2\, \rho_\infty U_\infty^2 t}$
L	characteristic length
M	Mach number
N	$\dfrac{\rho\mu}{\rho_w \mu_w}$
p	pressure
p_o'	pitot pressure
q	surface heat transfer rate
Re	Reynolds number
T	temperature
t	plate thickness
U	ambient velocity
u	velocity in boundary layer
x	Cartesian coordinate parallel to free-stream velocity
y	Cartesian coordinate perpendicular to free-stream velocity
z	variable defined in Appendix A, Eq. (A-10)
β	defined in Appendix B, Eq. (B-2)
γ	specific heat ratio
δ^*	displacement thickness

ϵ	inverse shock density ratio
ζ	defined in Appendix A, Eq. (A-10)
η	defined in Appendix A, Eq. (A-4)
θ	momentum thickness
K_ϵ	$\epsilon M_\infty^3 k \frac{t}{x}$
μ	viscosity
ξ	defined in Appendix A, Eq. (A-4)
ρ	density
ϕ	u/u_δ
$\bar{\chi}_\epsilon$	$\epsilon\left(0.664 + 1.73\, T_w/T_o\right) M_\infty^3 \sqrt{\frac{C_*}{Re_L}}$
$\bar{\chi}'$	$M_\infty^3 \sqrt{\frac{C_*'}{Re}} \left(\frac{T_\infty}{T_w}\right)^{\frac{1-\omega}{2}}$
$\bar{\chi}_\epsilon'$	$A\epsilon\left(0.664 + 1.73\, T_w/T_o\right)\bar{\chi}'$
ψ	angle of flow deflection
ω	exponent in temperature-viscosity law, $\mu \propto T^\omega$

Subscripts

o	reservoir condition
∞	free-stream conditions
w	wall condition
δ	evaluated at the boundary layer edge

I. INTRODUCTION

It has been recognized for sometime that thermochemical nonequilibrium processes occurring in the flowfield might have an appreciable effect on the aerodynamic characteristics of re-entry bodies. Their qualitative effects at various points in the flowfield were anticipated first from elementary energy considerations. Subsequent theoretical treatments have become available treating simple configurations in various models of air (for example Refs. 1-5) so that quantitative predictions of these effects can be made. However, experimental verification of these results are required to demonstrate their validity and to assess the importance of nonequilibrium effects in light of viscous effects. The purpose of this report is to present experimental surface pressure and heat transfer data obtained on a basic configuration, a flat-plate model with wedge leading edges. These measurements were made in the CAL hypersonic shock tunnels, with air as the test gas, at reservoir temperature ranging from 3300°K to 6600°K. They serve to demonstrate the magnitude of nonequilibrium effects as compared with viscous effects, and to test a simple method for analyzing the model flowfield.

A basic difficulty in high temperature experiments is in obtaining a comparison to demonstrate nonequilibrium effects. An ideal method would be to include experiments in which all gas-dynamic quantities were duplicated except, in one instance, the gas was equilibrated throughout the flowfield, and in another, the gas behaved ideally. This approach is very difficult owing to tunnel limitations. A more practical method is to select a model configuration for which the equilibrium, nonequilibrium, and ideal-gas solutions are available. The latter approach is used here.

The wedge leading edges were designed to have a strong, attached shock wave so that the thermal and chemical nonequilibrium in the shock layer could be predicted with normal shock wave solutions. The Prandtl-Meyer expansion at the juncture between the wedge leading edge and the flat plate afterbody serves effectively to quench the vibrational excitation and the chemical reactions, freezing a fraction of the total energy in these modes. The consequences of freezing out this fraction of the total energy can then be approximately determined by assuming the gas is frozen immediately in the expansion fan, and expands as an ideal-gas.

The two main elements in this model, the wedge flow and the Prandtl-Meyer expansion, are classical and have been studied in some detail in the literature. These serve as a certain justification for the elementary approach outlined above.

Wedge flows have been considered by a number of investigators beginning with Ivey and Cline[6] who applied Bethe and Teller's normal shock wave results for equilibrium air[7] to wedge flows. More recent work has been concerned with the relaxation process to the equilibrium state, and has included investigations by Moore and Gibson[8], Dressler[9], Sedney et al[10], Vincenti[11], Capiaux and Washington[12], South[13] and Lee[14]. All of these treat chemical or vibrational relaxation on a wedge within varying approximations, ranging from an analytic small-disturbance approach to a complex machine solution based on the method of characteristics. The important features of these investigations are to show that the shock wave angle is determined at the apex by locally frozen flow and approaches the equilibrium shock angle far downstream. Similarly, the pressure and velocity on the wedge face are always bounded by the frozen and equilibrium gas values, being quite insensitive to relaxation effects. This result partially justifies the present streamtube approach: to assume constant pressure and velocity on the wedge face and thereby reduce the problem to an equivalent normal shock wave problem. This approximation has been tested by Sedney et al[10], for the case of vibrational nonequilibrium, and shown to be in excellent agreement with the more exact solution.

The structure of a nonequilibrium Prandtl-Meyer expansion fan has been investigated in a similar fashion by Wood and Parker[15], Napolitano[16], Bloom and Steiger[17], Appleton[18], Glass and Kawada[19], Glass and Takano[20], and by Arave[21]. All of these investigate chemical relaxation in and following a Prandtl-Meyer expansion from a uniform, equilibrium state. These investigations are concerned with the relaxation process from the initially frozen state at the corner, to complete equilibrium far downstream, and are essentially in agreement on the gasdynamic relaxation effects. The one possible point of disagreement, on the existence of a recombination shock wave, appears to have been resolved by Glass and Takano[20] as stemming from the gas model. This is important to the present research since a secondary shock wave was observed in the flowfield near the expansion fan. The evidence indicates it was not a recombination shock since a recombination shock wave increases in intensity near the body.

The available solutions for wedge flows indicate that a streamtube calculation of the wedge flow is a good approximation for the vibration and chemical kinetics. These and the available solutions for Prandtl-Meyer flows shed no light on the accuracy of the approximation for the afterbody flow. It might be expected that there will be an effect stemming from the shock layer nonequilibrium at the leading expansion wave. There is no a priori basis for assessing this effect.

In the present research, the model was tested in air with a small-scale and a large-scale wedge leading edge, both at low temperature and high temperature conditions. The test with the small-scale leading edge at a low temperature served as an ideal-gas experiment, while the experiment at a high temperature tested one extreme of nonequilibrium in which the entire flowfield remained frozen. In the experiment with the large-scale leading edge at low temperature, it appears that the only excited mode was oxygen vibration and the results of this experiment are interpreted as showing the consequences of vibrational nonequilibrium. In contrast, the high temperature experiment with the large-scale wedge leading edge apparently produced both vibrational excitation and oxygen dissociation in the shock layer, and the results are interpreted as demonstrating the consequences of this nonequilibrium.

The aim in these experiments was to isolate the inviscid non-equilibrium effects. However, the first experiments indicated boundary layer displacement effects which were comparable with the nonequilibrium effects under investigation. Consequently, an important aspect of this research centered on isolating the boundary layer displacement effects from the nonequilibrium effects. In the experiments with the small-scale leading edge, it was found that a consistent correlation could not be obtained within existing ideal-gas similitude parameters which were based on a linear viscosity-temperature relation. These parameters were generalized to account for a non-linear viscosity-temperature relation (Appendix A) to show that the observed effects stemmed from this cause and not from thermochemical nonequilibrium.

In the experiments with the large-scale leading edge, a schlieren photograph indicated an unusually thick boundary layer on the afterbody, and the pressure data showed an unanticipated variation with distance. There are no boundary layer solutions for displacement effects when the boundary layer is processed by a Prandtl-Meyer expansion fan. Consequently, a matched similarity solution was formulated (Appendix B) to show that the observed variations in afterbody pressure, heat transfer, and boundary layer thickness were self-consistent. The same schlieren photograph showed a second shock wave embedded in the afterbody flowfield. This report consequently includes a review of certain literature on boundary layer flows at corners, as well as a momentum integral derivation (Appendix C) to demonstrate that the shock wave could result from the rapid boundary layer growth at the wedge shoulder.

The next section describes the experimental equipment and includes a description of the methods used to calculate the ambient stream conditions. The following section discusses the experimental results. The data obtained with the small-scale model are presented first. Following this, the data obtained with the large-scale model in low-temperature experiments are presented to isolate the gasdynamic effects. These are followed by a discussion of the data obtained with the large-scale model in high temperature experiments.

II. EXPERIMENTAL APPARATUS

MODEL

The model, Fig. 1, consisted of an instrumented slab with detachable leading and trailing edges. The slab instrumentation was comprised of thin film heat transfer gages and piezoelectric pressure transducers vented through surface orifices. The thin film heat transfer gages widely used by a number of investigators[22, 23] were used in conjunction with analogue networks[24] which converted the measured surface temperature to heat transfer rates. All gages were coated with a titantium dioxide film about 0.1 microns thick to electrically insulate them and to minimize catalytic heat transfer. Heat transfer gages were mounted on either side of the model centerline to provide a simultaneous check on the effects of a finite span. The data from these gages were in good agreement with that from the corresponding centerline gage.

The pressure transducers, described in Ref. 25, are diaphragm-type transducers, driving modified lead-zirconium-titanate crystals, with a nominal output of 2 volts/psi. It was found during the present research that the transducer was temperature sensitive, and under certain low density conditions would indicate negative pressures. It was concluded that this effect stemmed from the hot gas expanding the aluminum transducer diaphragm and two corrections were made. One was to build the transducer with an Invar diaphragm and the other was to cool the hot gas entering the transducer by passing it over a copper heat sink. It was found that either modification eliminated the negative signal and both indicated the same pressure level. The present experiments were made with both types of transducers spaced alternately along the model chord.

The model accepted either of two wedge leading edges, each with a wedge angle of 42-1/2°. This angle was selected to produce a strong attached shock wave under both ideal gas and equilibrium gas conditions. The first wedge was 1/2" thick (the same as the instrumented slab) and was selected, in keeping with the anticipated test conditions, to produce essentially no dissociation or vibrational excitation in the shock layer. This would correspond to the extreme case of nonequilibrium in which the flow does not relax from the ideal state.

The second wedge leading edge, shown in Fig. 1, was four inches thick and was designed to produce a significant level of dissociation and vibrational excitation in the shock layer. One pressure transducer was mounted on this wedge.

SHOCK TUNNELS

The wedge models were tested in both the CAL 4-ft. shock tunnel and the CAL 6-ft. shock tunnel. The former, described in Ref. 26, operates on the tailored interface principal with a heated helium driver. It operates with reservoir temperatures and pressures ranging up to about 3600°K and 400 atm. The CAL 6-ft. shock tunnel, described in Ref. 27, also operates on the tailored interface principle but with a heated hydrogen driver. It has recently been run with reservoir temperatures and pressure as high as 8000°K and 1300 atm. The present research was started before the full capabilities of the 6-ft. shock tunnel had been realized. In particular, it was found that the available test time decreased with increasing reservoir temperature, and the test time was about 200-300 microseconds with a reservoir temperature of 6600°K. This test time limitation was subsequently improved by lengthening the shock tube, and test times of about 1-2 milliseconds are obtained at a reservoir temperature of 6600°K.

Low temperature experiments were made in the test section of the 4-ft. shock tunnel, and the model was mounted on the cables shown in Fig. 1. This mounting system uses two cables at each of the model extremities which are connected to the test section wall with springs to isolate the model from tunnel vibrations. The high temperature experiments with the large-scale model in the CAL 6-ft. shock tunnel required the highest possible density. Consequently, the model was sting-mounted and tested near the 3-ft. diameter station in the nozzle. A standard pitot head was mounted on a bracket attached to the model lower surface to obtain a pitot pressure measurement.

AMBIENT TEST CONDITIONS

During each experiment, the speed of the incident shock wave and the reservoir pressure were measured in the shock tube, and the pitot pressure was measured at the model location. The reservoir conditions were then computed for equilibrium air using the measured shock speed and the shock tube conditions prior to the experiment. Any difference between the measured and the calculated reservoir pressure was assumed to be caused by isentropic wave processes.

The test section conditions for the low temperature experiments were determined by assuming the air was in thermodynamic equilibrium in the nozzle expansion. It was assumed that the expansion was isentropic, and the following hypersonic approximations were used,

$$U_\infty \approx \sqrt{2H_o} \qquad \rho_\infty \approx \frac{p_o'}{U_\infty^2(1-\epsilon/2)}$$

where H_o is the reservoir enthalpy, p_o' is the measured pitot pressure, ϵ is the density ratio across a normal shock wave, and ρ_∞ and U_∞ are the ambient density and velocity, respectively. The results of this procedure have been checked with exact numerical solutions and found to be accurate to within $\pm$ 0.4% over the range of test Mach numbers covered here.

The test section conditions for the high temperature experiments were determined, taking account of the nozzle nonequilibrium. The reservoir conditions were calculated as above, and used as input data for the CAL computer program for nonequilibrium nozzle expansions[28] under the assumption of vibrational equilibrium. The solution was terminated at the nozzle station where the computed and measured pitot pressures were equal.

The test gas was dry air obtained from the Matheson Company in East Rutherford, New Jersey. The gas was not analyzed for these experiments because prior mass spectrometer analyses of this product showed it to be free of detectable contaminants. A typical analysis for the gas showed the composition to be

Oxygen	21.05%
Nitrogen	77.93%
Argon	.97%
Carbon Dioxide	.05%

The hydrocarbon content, as indicated by acetone and alcohol, was less than 100 parts per million.

III. EXPERIMENTAL RESULTS

SMALL-SCALE MODEL

As noted in the previous section, the experiments included tests on the model fitted with a small-scale wedge leading edge. This experiment was intended to test one extreme of flowfield nonequilibrium in which the shock layer scale and density were such that no energy was lost in dissociation or vibration. Consequently, the gas should behave as an ideal gas throughout the flowfield, and the experimental data should be predicted by ideal gas theory. This ideal-gas limit was investigated by testing the small-scale model at high temperature conditions (T_o = 6600°K) and then repeating the experiment at the low reservoir temperature where the gas can be regarded as ideal. These experiments were made in a range where viscous interaction effects were significant. Consequently, it was necessary to maintain the same ratio of boundary layer displacement effects to nose bluntness effects between the two experiments. The theory of Ref. 29 was used as a guide to select the test conditions and to correlate the experimental data.

The theory of Ref. 29 is a zero-order theory treating the combined effects of boundary layer displacement and nose bluntness on a flat plate at zero angle of attack. It has been verified under low temperature conditions ($T_o \approx$ 2000°K) in the experiments of Hall and Golian[29, 30]. Within the theoretical limitations, the theory shows that the ratio of these two effects is unaltered if the parameter,

$$\frac{\bar{\chi}_\epsilon}{(K_\epsilon)^{2/3}} = \epsilon^{1/3}\left(0.664 + 1.73\, H_w/H_o\right)\left(x/kt\right)^{2/3} M_\infty \sqrt{\frac{C_*}{Re_x}}$$

is maintained constant. This criterion was used in selecting conditions for the high temperature and the low temperature experiments, but a consistent correlation was not obtained. These data are presented in Figs. 2 and 3, correlated in terms of the parameters given in Ref. 29. It can be seen that the pressure data from the two experiments correlate well within these parameters, falling below the theory. In contrast, the heat transfer data do not correlate within these parameters.

The possibility of vibrational relaxation has been checked by assuming that the air constituents relax like the pure gases; that is, without any cross-coupling between oxygen and nitrogen. The vibrational relaxation lengths have been calculated for the conditions in the wedge shock layer using Blackman's results for oxygen and nitrogen[31]. The low temperature experiment produced oxygen and nitrogen relaxation lengths of 20 and 1000 times the wedge length, respectively, indicating that these modes were not excited. The corresponding relaxation lengths for oxygen and nitrogen in the high temperature experiment were about 3 and 30 times the wedge length, respectively, implying that nitrogen vibration was not excited, but oxygen vibration was excited to about 22% of its equilibrium value. This corresponds to about 4% of the gas equilibrium vibrational energy, or about 1% of the gas static enthalpy in the wedge shock layer. Consequently, if this intuitive model is assumed, it appears that vibrational excitation was energetically unimportant in both experiments. Within the same framework, dissociation can be discounted on the grounds that the relaxation length was always greater than the vibrational relaxation length.

The behavior shown in Figs. 2 and 3 is not explained within the existing ideal gas theory[29] since the heat transfer is directly related to the pressure.

In particular, Cheng[29] shows that the heat transfer should vary as

$$M^3 C_H = 0.332\, M^3 \sqrt{C_* / Re_L}\; \frac{p/p_\infty}{\sqrt{\int_0^L \frac{p}{p_\infty} \frac{dx}{L}}}$$

Consequently, the scatter in heat transfer between the two experiments should be less than the scatter in the pressure data.

It is believed that the lack of correlation in heat transfer, Fig. 3, stems from the fact that certain of the theoretical assumptions were violated in the present experiments. In particular, an important assumption in Cheng's theory is that the viscosity varies linearly with temperature. This, of course, is a good assumption at low reservoir temperatures where the temperature in the boundary layer does not exceed 300-500°K. However, the boundary layer temperatures in the present experiments ranged as high as 1500°K, and the assumption of a linear viscosity-temperature relation is open to serious question. In order to check on this assumption, the theory of Ref. 29 was formulated to allow for a viscosity temperature relation, $\mu/\mu_\infty = C_*'(T/T_\infty)^\omega$. This formulation, given in Appendix A, was pursued to the point of identifying the governing parameters.

The pressure and heat transfer data shown in Figs. 2 and 3 have been cast into the similarity variables given in Appendix A, Eqs. (A-17) and (A-18), and are shown in Figs. 4 and 5. In making these plots, it was assumed that A = 1.0 (Eq. (A-8)) and Cheng's theory[29], included for comparison, assumes ω = 1.0. The viscosity exponent was determined for each of the experimental conditions by matching Sutherland's formula for the viscosity over the range of temperatures encountered in the flowfield. Comparing Figs. 2 and 3 with Figs. 4 and 5, it can be seen that the modified similarity variables have not changed the correlation for the pressure data appreciably except to move the data parallel to the theory. The pressure data still fall about 50% below the theory. In contrast, the modified similarity parameters have improved the heat transfer correlation and brought the high temperature and low temperature data into good agreement.

It should be emphasized that these correlations cannot be used to conclude that the assumption, $A = 1$, is valid. On the contrary, it seems likely that $A \neq 1$, and that the good correlation results from the fact that the viscosity exponent varies little between the two experiments and the influence of the wall temperature ratio is small. The correlations do indicate that the flow field for the high temperature experiment was, for practical purposes, entirely frozen, and the gas behaved as an ideal gas.

LARGE-SCALE MODEL

It was noted in the previous section that a model with a 4-inch thick wedge leading edge was tested at high and low stagnation temperatures. A common feature in all of these experiments was the thick boundary layer on the afterbody with attendent displacement effects on pressure and heat transfer. These effects could not be predicted because there are no theoretical methods for predicting the boundary layer growth including the Prandtl-Meyer expansion fan at the wedge shoulder. A simplified boundary layer analysis was made in the present research to demonstrate that the observed variations in afterbody pressure and heat transfer stemmed from boundary layer displacement effects. This analysis, presented in Appendix B, establishes a basis for interpreting the experimental data.

Chronologically, the experimental program consisted of high temperature experiments, followed by low temperature experiments to investigate boundary layer displacement effects under conditions where dissociation would not be important. The high temperature experiments were repeated, following shock tunnel modifications*, to verify the original experiments. The data obtained at low temperatures will be presented first in order to isolate boundary layer effects common to both experiments. Following this, the high temperature data will be discussed.

Low-Temperature Experiment

The purpose of the low-temperature experiment was to investigate the gasdynamics, especially the boundary-layer displacement effects, in the wedge experiment without the complications due to chemical relaxation effects. Consequently, the low temperature experimental conditions were selected so as to produce approximately the same boundary layer thickness at the wedge shoulder as in the high temperature experiments; that is, the same Mach number and Reynolds number at the wedge shoulder. This test was performed in the CAL 4-ft. shock tunnel with a reservoir temperature of 3300°K and a reservoir pressure of 260 atm. The measurements included surface heat transfer, pressure, and schlieren observations of the flowfield.

The experimental results, presented in Figs. 6, 7, and 8, show several important effects. First, one would expect that for the inviscid, ideal-gas case, the first expansion wave reflecting from the shock wave should impinge on the afterbody at $x/t \approx 3.2$. Consequently, the experimental pressure data corresponding to $x/t < 3.2$ should be invariant with chord-

*These were scheduled modifications to extend the shock tunnel performance and to increase the available test time.

wise station. Similarly, if one neglects the boundary layer on the wedge face, the heat transfer on the afterbody would be expected to vary inversely as the square root of distance from the wedge shoulder for $x/t < 3.2$. The experimental data, Figs. 6 and 7, show that the afterbody pressure varied by a factor of about 2, contrary to expectations, but the heat transfer varied approximately as expected.

A second item to be noted is shown in the schlieren photograph, Fig. 8, the thick boundary layer on the afterbody. The boundary layer thickness on the wedge face is indiscernible in the schlieren photograph but is estimated to be about 1/10 the thickness of the afterbody boundary layer. The afterbody boundary layer thickness varies slowly with distance, being about 0.6 inches thick, 0.6 inches from the wedge shoulder, and being about 0.8 inches thick, 8 inches from the shoulder. The third effect to be noted, Fig. 8, is the distinct change in the bow wave angle about half way up the wedge face. The fourth feature in Fig. 8 is the secondary shock wave in the flowfield. Each of these four effects will be discussed in the succeeding paragraphs.

Boundary-Layer Displacement Effects. The pressure data in Fig. 6, coupled with the schlieren photograph of the model flowfield, strongly suggest that the observed behavior in the afterbody pressure and heat transfer stem from boundary layer displacement effects. This hypothesis can be checked by comparing the data with the matched similarity solution outlined in Appendix B. This comparison was made by matching the solution to the measured pressure, heat transfer, boundary layer displacement thickness, and pressure gradient at $x/t = 1.3$. The computed results are compared with the pressure and heat transfer data in Figs. 6 and 7, respectively, and with the boundary layer thickness, as measured from the schlieren photograph, in Fig. 8. The matched similarity solution predicts the observed variations in pressure, heat transfer, and displacement thickness with good accuracy, thereby indicating that the observed behavior stems from the displacement effect of the boundary layer. This conclusion will be strengthened further by subsequent comparisions.

Asymptotic Afterbody Pressure. The above discussion on boundary layer displacement effects is buttressed somewhat by the comparison of the pressure measured at downstream stations on the afterbody with theoretical estimates which neglect the boundary layer effects. The data and the matched similarity solutions indicate that the rate of growth of the boundary layer is small at $x/t \approx 2.0$, and that the pressure measured at this station can be interpreted as the inviscid pressure.

The method used to compute the afterbody pressure was to calculate the condition at the shoulder on the wedge face, taking account of source flow effects[32], and to assume that in the subsequent Prandtl-Meyer expansion, the gas remained vibrationally and chemically frozen at the shoulder conditions. Three cases were considered for the gas on the wedge face: (1) an ideal-gas, (2) an equilibrium gas, and (3) a gas in which the inert degrees of freedom were partially excited. The first two cases represent the two extreme nonequilibrium limits, while the third is intended to approximate the actual condition. The nonequilibrium condition was estimated by assuming again that the oxygen and nitrogen in the air relax as the pure gas. It is recognized that the present theoretical understanding of air thermochemistry is quite poor, and this model is intuitive. It assumes that there is no vibration-vibration coupling between oxygen and nitrogen, and that oxygen-nitrogen collisions are as efficient as oxygen-oxygen or nitrogen-nitrogen collisions in the relaxation process. It is used for lack of a better model. The calculation was made, using Blackman's data for vibrational relaxation[31], by noting that the most important relaxation process occurring on the wedge face is O_2 vibration which has a characteristic relaxation length about 1/4 the length of the wedge face under these test conditions. The corresponding characteristic length for N_2 vibration is about twelve times the length of the wedge face. Consequently, the shoulder conditions should be approximated by the assumption that O_2 is vibrationally equilibrated while N_2 remains frozen.

The asymptotic pressure levels computed for these three cases are indicated in Fig. 6. The computation for an ideal gas and that for a frozen expansion from equilibrium conditions on the wedge face differ by a factor of about 2-1/2. This illustrates the magnitude of the nonequilibrium effect which could exist at these low temperature conditions, depending on model scale and ambient density. The elementary model for vibrational non-equilibrium is seen to be in good agreement with the pressure data, falling somewhat above the data. This agreement tends to substantiate the hypothesis that the observed decay in afterbody pressure stems from boundary layer displacement effects.

It should be noted that the pressure decay in Fig. 6 cannot be explained as a vibrational relaxation effect. Assuming the above elementary model for vibration applies, it is easy to show that vibration is almost entirely frozen within the first 5-10° of the Prandtl-Meyer expansion.

Consequently, any relaxation on the afterbody would tend to remove energy from the vibrational mode, and increase the pressure toward the ideal gas limit. It is estimated that the characteristic length for vibrational relaxation on the afterbody is 227 feet.

Bow Wave Curvature. The schlieren photograph, Fig. 8, shows that, in this low temperature experiment, the oblique shock wave on the wedge face was not straight. There is a distinct bend in the bow wave at about the center of the wedge face. Using an estimated boundary layer growth rate $\frac{d\delta^*}{dx} \approx \frac{1}{2}^\circ$ on the wedge face, it is found that the shock angle near the wedge vertex is in good agreement with that calculated for an ideal gas, and the shock angle on the aft portion of the wedge is in good agreement with that calculated for an equilibrium gas. This behavior suggests that a vibrational relaxation process is taking place in the shock layer, but the fact that the shock angle quickly adjusts to the equilibrium angle does not necessarily imply that the shock layer is equilibrated. This behavior can be qualitatively understood from Moore and Gibson's analysis[8]. That work considers the chemical relaxation process for a wedge in supersonic flow using small disturbance theory. They show that near the wedge vertex, the disturbance is centered on the frozen Mach line. The strength of this disturbance decays with distance from the vertex, and the disturbance develops into a dispersed wave centered on the equilibrium Mach line. The fact that a dispersed wave is not evident in Fig. 8 probably results from the schlieren apparatus being insensitive to weak waves.

The agreement between the observed wave angle and the equilibrium wave angle must be regarded as somewhat fortuitous since the source flow effect tends to decrease the wave angle. Hall's source flow correction[32] has been applied here using the second-order relation in y/R_o to estimate the maximum effect on the shock wave angle at the wedge shoulder. This correction would account for about half the difference between the equilibrium and the frozen wave angle. It should be emphasized, however, that this is a maximum source-flow effect since the calculation assumes the geometric y/R_o applies. Recent measurements in the 6-ft. shock tunnel* at twice the Reynolds number of the present experiments show that this is conservative. The applicable y/R_o at that test Reynolds number was about 2/3 the geometric value. This suggests that the source flow effect in the present experiment should account for less than 1/3 the difference between the equilibrium and the frozen wave angle.

Secondary Shock Wave. One effect disclosed by the schlieren photograph, Fig. 8, is the presence of a secondary shock wave in the flowfield between the bow wave and the model. This shock wave does not appear to contact the body surface, suggesting that it results from a system of weak compression waves. Extrapolating the shock wave position to the model surface, it appears that the wave stems from some phenomenon occurring near the shoulder of the wedge.

At first glance, it would appear that this wave resulted from boundary layer separation at the wedge shoulder. The apparent separation bubble at the shoulder is actually an illusion. The upstream edge of this apparent bubble

---

*These measurements were made by J. A. Bartz in research sponsored by the AFOSR Mechanics Branch, Contract No. AF 49(638)-1433.

is the shoulder expansion fan. The downstream edge of the apparent bubble is actually a flaw in one of the schlieren windows, and if that spot is ignored, it can be seen that there is no separation bubble. Instead, it appears that the wave results from the rapid expansion and thickening of the boundary layer in flowing around the wedge shoulder.

The flow of a compressible boundary layer around a convex corner has received increasing attention in recent years, and there are presently a number of approximate techniques for estimating various aspects of the boundary layer behavior.

One approach to the problem, that of Hunt and Sibulkin[33], makes use of momentum integral techniques to determine the change in momentum thickness and displacement thickness around the corner. In obtaining this solution, it is implicitly assumed that the boundary layer profiles are similar on either side of the corner. In addition, it is assumed that the profiles are well represented by a power law, $u/u_\delta = (y/\delta)^{1/n}$. It is recognized that both of these are poor approximations. Nevertheless, this theory predicts about 75% of the displacement thickness observed in the schlieren photograph. Consequently, it can be used with some confidence to examine the rate of growth of the boundary layer around the corner. This has been done by dividing the corner expansion into 4° increments and computing the displacement thickness along the rays of the expansion fan. The boundary layer slope was then compared with the local flow direction to determine if they were consistent with an expansion wave. It was found that in the first 15-20° of the turning process, an expansion wave was not consistent with the boundary layer slope, and that a system of compression waves was indicated. This implies that the secondary shock wave observed in

Fib. 8 could be caused by the rapid initial thickening of the boundary layer in flowing around the corner.

Another approach to the problem of a viscous corner flow, that of Weinbaum[34], is to regard the flow in the immediate vicinity of the corner as an inviscid nonuniform flow, and to investigate the turning process with a wave diagram. A fundamental aspect of this procedure is that the boundary conditions far downstream specify that there be no normal pressure gradient and that all streamlines be parallel. These boundary conditions can be satisfied only if there is a wave reflected from the intersection of an expansion wave with entropy gradients. The sign of the wave depends on the Mach number before the expansion, and the reflected wave is compressive for $M < \sqrt{2}$. A basic difficulty in this procedure is that there is no method to account for the subsonic layer. The assumption used in Ref. 34 is that the streamline corresponding to an initial Mach number, $M = 1$, remains parallel to the surface in the expansion, and that the family of compression waves reflect from this streamline. The surface of interest is that along which the Mach number is unity since the compression waves will be reflected from this surface. It is not clear what shape this surface will have, but if that surface is concave, the family of compression waves would coalesce to form a shock wave.

Finally, there is a third approach to the problem, that of Stroud[35], which is based upon the momentum integral technique and is applied to a curved wall. The aim in this approach is to investigate the boundary layer response to a discontinuity in surface curvature. Stroud's approach has been modified in Appendix C to show that the boundary layer will always tend to produce a locally compressive flow at a convex corner. This conclusion is qualitatively verified by the boundary layer calculation included as an appendix to Wagner and Watson's work.[44] Interest there centers on bodies of revolution with contoured noses; that is concial noses with a constant-radius fairing between the nose and afterbody. The aim is to show that, for practical purposes, the boundary layer growth begins at the afterbody shoulder. This computation shows the boundary layer thickens rapidly near the afterbody shoulder, producing a locally compressive corner in the displacement thickness. This implies that a system of compression waves, and hence a second shock wave, should be present in these flow fields.

To summarize the available theoretical literature, the problem of a boundary layer flow around a convex corner is approached from different viewpoints. However, all these approaches qualitatively indicate that compressive waves are generated in this flow field. These analyses tend to substantiate the hypothesis that the observed secondary shock wave stems from the boundary layer negotiating the convex corner.

High Temperature Experiments

Three high temperature experiments were performed in the CAL six-foot hypersonic shock tunnel. The reservoir and calculated ambient conditions are summarized in Table 1. The pressure data are shown in Figs. 9, 10, and 11. As expected, a large decay in afterbody pressure was found which is similar to that obtained in the low temperature experiments. The heat transfer data, shown in Fig. 12, also displays the same qualitative behavior as the low temperature data. In all cases, the matched similarity solutions predict the trend of the data, indicating that the observed variations stem from boundary layer displacement effects.

The theoretical asymptotic pressure levels in Figs. 9-11 were calculated using the air models indicated in the figure and assuming vibration and dissociation were frozen in the shoulder expansion. The theoretical afterbody pressures are bounded above by the ideal gas prediction and below by that for a frozen expansion from equilibrium flow. The corresponding values for complete equilibrium, a frozen expansion from a vibrational and chemical nonequilibrium flow, and a frozen expansion from a vibrational equilibrium but chemical nonequilibrium flow are shown within the two bounding values. The details of these calculations are given in the succeeding sub-section.

The pressure data, Fig. 9, show a sizeable nonequilibrium effect in the sense that sufficiently far from the shoulder the pressure appears to approach a constant value which is significantly below the equilibrium level. This "asymptotic" pressure level lies between the two theoretical levels which represent likely limits, lines 7 and 8. That is, the pressure is less than that predicted for the freezing of the vibrational and chemical nonequilibrium model, but greater than that for freezing of the vibrational equilibrium-chemical nonequilibrium model. In the first experiment, the data are closer to the results of the first model, and in fact are below it by about only 10 to 15%. It should be noted that the vibrational model has a significant effect on the afterbody pressure, the levels differing by almost a factor of 2.

The conditions in test number 2 are somewhat different than for test number 1 (see Table 1). In particular, the reservoir temperature is somewhat lower, the reservoir pressure is lower by about a factor of 1.6, and the ambient density is greater by about a factor of 2. The effect of increased density is to reduce the relaxation lengths for all processes on the wedge face by about a factor of 2. Consequently, one would expect that more energy would be frozen out in the corner expansion with the result that the afterbody pressures would be reduced from those in the first experiment. Furthermore, since the increased pressure will tend to suppress the equilibrium dissociation level, one might suspect that vibration would assume a greater role in this experiment. This is reflected in the large effect that the vibrational model has on the afterbody pressure; a factor of about 2.5 in this case. Once again, the data indicate an asymptotic level which is bracketed by the two likely theoretical levels.

The reservoir conditions of experiment number 3 are close to those of experiment number 2. However, in this case the model was placed further downstream of the throat at a position where the ambient density was about 10% higher than that for test number 1. The increased density promotes equilibration, and one would expect that the afterbody pressures for vibrational equilibrium and nonequilibrium would be in better agreement than in the first test. This turns out to be the case. In fact, the difference between these two levels is only about 15% in this case. Again, the data are bracketed by these values.

The heat transfer data which were obtained are shown in Fig. 12. A large heat transfer decay is indicated, the trend of which in all cases is predicted quite well by the matched similarity solution. Little further can be said about the heat transfer since there is no complete boundary layer solution accounting for the wedge shoulder. The heat transfer data do reflect the nonequilibrium effects on the pressure through the parameter, $\beta = \frac{1}{p} \frac{\partial p}{\partial x}$, in the matched similarity solution. However, the pressure data are a more definitive test of these effects. Consequently, the remaining paragraphs will deal with the afterbody pressure. In particular, the next sub-section will describe the theoretical methods used to calculate the afterbody pressure, including an assessment of the vibrational model and a discussion of some of the vibrational coupling effects. The assumption that the air is frozen immediately in the shoulder expansion fan is considered both within the context of Blackman's rate data and within the context of the more recent data of Hurle, Russo and Hall. Following this, attention is given to possible inviscid sources of the pressure decay on the afterbody to show that neither source flow effects or nonuniformities in the shock layer due to nonequilibrium could account for the behavior. Finally, the effects of nozzle nonequilibrium are considered to indicate that they should have a small effect on afterbody pressure.

Theoretical Calculation of Asymptotic Afterbody Pressure. The first step in determining the afterbody pressure involves the calculation of the condition immediately behind the shock at wedge apex. These calculations were performed for given free stream conditions by iterating on ϵ , the inverse shock density ratio, and imposing the condition that the flow be parallel to the wedge surface. The conditions corresponding to different air models were calculated by using the appropriate state relations.

The effects of thermo-chemical nonequilibrium along the surface of the wedge were calculated using a streamtube method by which the equivalent normal shock problem was solved using a CAL machine program[36, 37]. The chemical model used in this computation is given by the following reactions.

1.)	$O_2 + M \rightleftharpoons 2O + M$	4.)	$N + O_2 \rightleftharpoons NO + O$
2.)	$N_2 + M \rightleftharpoons 2N + M$	5.)	$O + N_2 \rightleftharpoons NO + N$
3.)	$NO + M \rightleftharpoons N + O + M$	6.)	$N + O \rightleftharpoons NO^+ + e^-$

This model is the same as used in Refs. 36 and 37 except that the reaction

$$N_2 + O_2 \rightleftharpoons 2NO$$

has been deleted. The machine solution for the present conditions showed that this reaction was unimportant. The computed species concentrations are given in Table II both for the ambient stream and at the wedge shoulder for a typical experimental condition. The normal shock calculations were performed with two different vibrational models in order to assess the possible role of vibrational relaxation along the wedge. In the first, all species were assumed vibrationally equilibrated. In the second, O_2 and N_2 were allowed to relax vibrationally according to the rates given by Blackman[31] while NO equilibrium was specified. This model is justified to a certain extent in the sense that the extrapolation of the data of Wray[38] for Ar-NO mixtures to pure NO indicates that the vibrational relaxation length of NO is the order of 1/50 of the length of the wedge face for the conditions on the wedge face while that of O_2 and N_2 is comparable to the wedge dimension. The correctness of this length rests on the assumption that all species are at least as effective as NO in equilibrating NO vibration, which is consistent with the use of the Blackman rates for N_2 and O_2.

The no-coupling assumption may not be justifiable. A numerical check has indicated that the type of vibration-dissociation coupling discussed by Treanor and Marrone[39] for pure O_2 and N_2 plays no role in these experiments. Another coupling mechanism is that proposed by Bauer and Tsang[40] which involves exchange reactions and tends to increase the rate of vibrational equilibration. If this were an important effect, then the model employed here would under-estimate the vibrational excitation and over-estimate the afterbody pressure. In any case, the difference between the afterbody pressure predicted for vibrational nonequilibrium and that for vibrational equilibrium should indicate the possible pressure deviation which can arise from these coupling effects on the wedge face. It is recognized, of course, that other coupling mechanisms could be present. There is presently no known basis for estimating these effects.

For the conditions of these experiments the energy of dissociation and vibration are approximately equal and together comprise approximately 20% of the total enthalpy when vibrational equilibrium is very rapid. The static enthalpy is about 50% of the total enthalpy on the wedge face. Consequently, if the corner expansion is sufficiently fast, about 40% of the static enthalpy will be frozen which would be expected to greatly affect the afterbody pressure.

When vibrational relaxation is allowed, the temperature is initially higher, causing the dissociation rates to be higher than in the vibrational equilibrium case. The result is that the energy in dissociation is increased somewhat while the energy in vibration is reduced substantially. Consequently, the total energy which can be frozen out in the expansion is less than in the vibrational equilibrium case.

Source flow corrections to the theoretical shoulder conditions were calculated using the theory of Ref. 32. For the high temperature series the source-flow correction* to the afterbody pressure ranges from 20% to 34%,

---

*To apply the theory of Ref. 32, it is necessary to know the value of $\mathcal{R}_o$, the distance from the throat to the leading edge of the model. The following values were used:

High temperature test No. 1:	$\mathcal{R}_o$ = 9.75 ft.
High temperature test No. 2:	$\mathcal{R}_o$ = 7.50 ft.
High temperature test No. 3:	$\mathcal{R}_o$ = 10.23 ft.
Low temperature test:	$\mathcal{R}_o$ = 11.65 ft.

depending on the test conditions and the theoretical model for the wedge flow. The correction for the low temperature test was about 15%.

The amount of energy recovered in the expansion fan can be estimated by calculating the relaxation lengths of the various thermo-chemical processes and comparing them with the particle path lengths through the expansion fan. The longest path length belongs to the streamline which passes through the intersection of the shock wave and the leading characteristic from the corner. Clearly, the flow along streamlines near the body will be frozen if it is frozen along the longest streamline. The estimate was made by using the post-shock conditions corresponding to the vibrational equilibrium case.

The relaxation lengths for oxygen and nitrogen vibration were calculated at the shoulder and compared with the path length corresponding to a turning angle of 5°. On this basis, it can be shown that nitrogen vibration freezes almost immediately. However the oxygen relaxation length is comparable to the path length, although greater, so that it appears that some of the oxygen vibrational energy is recovered. The amount of energy recovery can be estimated by computing the effective specific heat ratio for the first 5° by assuming that nitrogen vibration is frozen while oxygen is equilibrated. Then the conditions along the characteristic corresponding to a 5° turn can be computed, including the local oxygen relaxation length. This process can be repeated for any number of angular changes. In this way, it was determined on the basis of Blackman's relaxation data that oxygen was definitely vibrationally frozen after about a 10° turn. Since the characteristic times for dissociation are greater than those for vibration, the chemical processes would also be frozen almost immediately.

The vibrational energy which might be recovered can be estimated by assuming that oxygen was vibrationally equilibrated during the first 10° of the expansion while NO was equilibrated during the entire expansion. In this way it was found that less than 14% of the vibrational energy was recovered. Consequently, it appears that less than 7% of the energy in vibration and dissociation would be recovered in the corner expansion. This represents a maximum recovery of about 3.5% of the static enthalpy.

Recently, experimental data have been obtained which appear to indicate that vibrational equilibration may proceed at a significantly higher rate in expansion-flow environments than in a post-shock flow[41]. In particular, it was shown that the N_2 relaxation rate in a nozzle expansion was at least 15 times the value reported by Blackman.

The implication of this result on the energy recovery in the corner expansion was investigated by increasing the relaxation rates of O_2 and N_2 by a factor of 15 and repeating the calculation discussed above. This time N_2 and O_2 vibration was not frozen until the flow expanded through an angle of about 20° and 35°, respectively. A conservative estimate indicated that, at most, 30% of the initial vibrational energy would be recovered. This is about 15% of the total energy in inert modes and about 7.5% of the pre-corner static enthalpy. Therefore even if the rates are significantly larger than those given by Blackman, it would appear that the asymptotic afterbody pressure would not be significantly affected.

Inviscid Sources of the Pressure Decay. It should be pointed out that the pressures determined by the method of the preceding section are valid predictions only up to the point on the body where the reflection of the leading characteristic from the shock intercepts the body. Consequently, source flow effects on the pressure in this region are determined by the effects at the shoulder, e.g., the change in shoulder pressure and Mach number. Physically, this simply means that information about source flow effects are communicated to the body by the characteristics which run to the body from the leading characteristic of the expansion fan. If conditions along the leading characteristic are uniform, then the source-flow correction must be a constant along the body up to the point where the wave reflection from the shock reaches the body.

It can be shown that the region in which the pressure measurements were made is affected by the conditions along only the first half of the characteristic originating at the shoulder. Therefore the uniformity of the source flow correction to the pressure in the region immediately aft of the corner where measurements were made is controlled by the uniformity of conditions along only the first half of the characteristic. The Newtonian theory of Ref. 32 was used to conservatively estimate the change of conditions along this line. It was found that the pressure differs by only about 1.5% which implies that the velocity must be uniform to about .3%. Therefore the source flow correction to the afterbody pressure should be very nearly a constant in the region where pressure measurements are made.

The flow on the wedge face is basically a two-dimensional flow since the vibration and chemical state vary between adjacent streamlines. It can be shown that the pressure along the leading characteristic cannot be affected more than about 12%. This implies that the velocity increases by a maximum of about 3%. The temperature at the midpoint of the leading characteristic can be obtained from the numerical results by reducing the length scale by a factor of two. In this way, it was found that the temperature increases by less than 8% between the corner and the midpoint of the leading characteristics, even in the most severe case considered. These results imply a reduction in Mach number which is at most about 1%. Thus it appears that thermochemically caused nonuniformities can be responsible for afterbody pressure deviations in the region of interest which are at the most the order of 10%, which is the order of the experimental error. Furthermore, this would be an effect which would tend to increase the afterbody pressure rather than cause a decay such as that which is observed.

Consequently, the combined effect of these inviscid mechanisms, which might produce a pressure deviation from a constant value, does not appear to be of sufficient magnitude to explain the observed pressure decay. This lends added weight to its interpretation as a viscous interaction effect.

Effect of Nozzle-Flow Nonequilibrium. Previous estimates[42] of the effect of nozzle airflow chemistry suggested that the free-stream atom concentration had a powerful effect on the afterbody pressure. Since this was an unexpectedly large effect and the calculations were based on some numerical extrapolations and approximations, the problem was examined more exactly in the present work in order to determine if the effect was real or simply a result of numerical inaccuracies. In particular, a detailed numerical solution for the nozzle flow was obtained, and the corresponding wedge flow calculations were performed with the ambient chemical composition as an input. The machine program for the nozzle flow used the same reactions as the normal shock wave program (page 25) except that the reaction, $N_2 + O_2 \rightleftharpoons 2NO$, was included and vibration was always assumed to be equilibrated. The afterbody pressure was calculated by the method described above and compared with that calculated in the same manner for an equilibrium nozzle flow. The results indicated that the afterbody pressures are in disagreement by only a few percent for both vibrational models, indicating that the previous estimates over-predicted the effects of free-stream dissociation. Hence it appears that the present experiments were largely insensitive to ambient dissociation. This is not to imply, however, that ambient dissociation will not be important under different conditions or with a different model.

Vibrational nonequilibrium in the nozzle flow has not been accounted for. However, recent experimental evidence[41] suggests that vibration equilibrates much more rapidly than expected in expansion-flow environments. Consequently, the energy which is ultimately frozen in the vibrating modes may be characterized by a relatively low vibrational temperature. This temperature has been calculated by considering the relaxation times in these experiments, and is conservatively estimated to be about 1600°K. This results in a frozen vibrational energy which is about 50% of the static enthalpy at the model station. Therefore, a relatively large effect should appear in static pressure and temperature. However, these quantities have a negligible influence on the rate processes on the wedge face when the free stream Mach number is large. Immediately behind the shock, the energy in vibration is only about 1% of the static enthalpy. Consequently, one would expect that the vibration rate processes on the wedge face would not be greatly effected by the vibrational energy frozen in the free stream.

CONCLUDING REMARKS

The experiments with a flat plate fitted with wedge leading edges have demonstrated several high-temperature effects. The tests with a small-scale model were made at a high reservoir temperature, but with an ambient density such that the flow field was essentially frozen. The data show that a consistent correlation between these high-temperature data and low-temperature data requires that a nonlinear temperature-viscosity relation be used in formulating the similarity variables.

The experiments with the large-scale model at a low temperature (3300°K) were made with an ambient Mach number and Reynolds number that would produce essentially the same boundary layer characteristics as in subsequent high-temperature experiments, but with minimum real-gas effects. This experiment showed that the expansion at the wedge shoulder caused the boundary layer to thicken rapidly to a thickness about ten times greater than that on the wedge face. This rapid thickening led to large displacement effects on the afterbody and evidently produced compression waves which formed a second shock wave within the flow field.

The calculations indicated that the gas temperature produced in the shock layer in the above experiment was sufficient to equilibrate oxygen vibration. In this case, the measured afterbody pressure was about 25% less than the ideal gas value. This result agrees reasonably well with that predicted using an equivalent nonequilibrium normal shock-wave solution for the wedge shock layer, and by assuming the flow to be frozen in the shoulder expansion.

The experiments with the large-scale model at high temperatures (6600°K) showed the same displacement effects as the low-temperature experiments, and larger effects due to flow field nonequilibrium. In this case, the calculations indicated that both vibration and dissociation were partially excited, with the energy in each mode being about equal. This led to an afterbody pressure about 35% below the ideal-gas value. These data fell between the theoretical results obtained with two nonequilibrium gas models. One model assumes nonequilibrium dissociation and vibration on the wedge face; the other nonequilibrium dissociation with vibrational equilibration on the wedge face.

APPENDIX A

THE EFFECT OF A NONLINEAR VISCOSITY TEMPERATURE RELATION ON COMBINED BLUNTNESS AND DISPLACEMENT

The basis for the present generalization stems from Cheng's analysis for the laminar boundary layer[29]. In particular, he shows that for unit Prandtl number, for a linear viscosity-temperature relation, for $\frac{\gamma-1}{\gamma+1} << 1$, and for hypersonic small disturbances, the governing momentum and energy equations reduce to the Blasius equation. If the viscosity relation,

$$\frac{\mu}{\mu_\infty} = C_*'\left(\frac{T}{T_\infty}\right)^\omega \qquad C_*' = \frac{\mu_*}{\mu_\infty}\left(\frac{T_\infty}{T_*}\right)^\omega \tag{A-1}$$

is introduced, these equations become

$$\left(N\phi_{\eta\eta}\right)_\eta + \phi\phi_{\eta\eta} = 0 \quad (N\theta_\eta)_\eta + \phi\theta_\eta = 0 \tag{A-2}$$

with the boundary conditions,

$$\eta = 0, \ \phi = \phi_\eta = \theta = 0 \qquad \eta \to \infty \ \ \phi_\eta = \theta = 1 \tag{A-3}$$

where

$$\phi_\eta = \frac{u}{u_\delta}, \quad \theta = \frac{H - H_w}{H_o - H_w}, \quad \eta = \frac{u_\delta}{\sqrt{2\xi}}\int_o^y \rho\, dy, \quad \xi = \int_o^x \rho_w \mu_w u_\delta\, dx$$

$$N = \frac{\rho\mu}{\rho_w\mu_w} = \left[\frac{T_w/T_o + \theta\left(1 - T_w/T_o\right) - \phi_\eta^2}{T_w/T_o}\right]^{\omega-1} \tag{A-4}$$

Certain conclusions can be reached from this system of equations. First, it can be seen from Eqs. (A-2) and (A-3) that the transformed velocity and enthalpy profiles are identical as long as the wall temperature is constant. Second, the transformation leads to a set of similarity variables for a given wall temperature ratio and a given value of the exponent, ω. Consequently, it can be expected that a consistent correlation between experimental data will be obtained within the variables given by Eq. (A-4) so long as the effect of the wall temperature ratio and the exponent, ω, do not vary appreciably between experiments.

The applicable correlation parameters are obtained by paralleling Cheng's calculation for surface heat transfer and pressure. Using the variables defined by Eq. (A-1)-(A-4), the displacement thickness becomes

$$M_\infty \frac{\delta^*}{L} = M_\infty \int_0^\infty \left(1 - \frac{\rho u}{\rho_\delta u_\delta}\right)\frac{dy}{L}$$

$$= A \bar{\chi}_\epsilon \left(\frac{T_\infty}{T_w}\right)^{\frac{1-\omega}{2}} \sqrt{\frac{C_*'}{C_*}} \; \frac{\sqrt{\int_0^L \frac{p}{p_\infty}\frac{dx}{L}}}{p/p_\infty} \qquad \text{(A-5)}$$

where A is a constant determined from Eq. (A-2).

$$A = \frac{\sqrt{2}\int_0^\infty \left[\frac{T_w}{T_0} + \phi_\eta\left(1 - \frac{T_w}{T_0}\right) - \phi_\eta^2\right] d\eta}{\left[0.664 + 1.73 \; T_w/T_0\right]} \qquad \text{(A-6)}$$

For the case where, N = 1, A = 1.

Cheng[29] determines the surface pressure using the Newton-Busemann relation for a curved shock wave

$$\frac{p}{p_\infty} = \gamma M_\infty^2 \,(y y')' \qquad \text{(A-7)}$$

where y is the vertical location of the shock wave from the surface and the prime indicates differentiation with respect to the x-coordinate. The momentum balance for the flowfield yields the following relation for the shock wave coordinates at zero angle of attack.

$$\left[y-\delta^*\right](yy')' = \epsilon k \frac{t}{2} \qquad \text{(A-8)}$$

where t is the body thickness and $k = \dfrac{D_N}{\frac{1}{2}\rho_\infty U_\infty^2 t}$ is the nose drag coefficient. Combining Eqs. (A-5), (A-7), and(A-8) leads to the following differential equation for the shock wave coordinates.

$$2y(yy')' - A\frac{\bar{\chi}_\epsilon\sqrt{L}}{M_\infty^2}\left(\frac{T_\infty}{T_w}\right)^{\frac{1-\omega}{2}}\sqrt{\frac{C_*'}{C_*}}\sqrt{yy'} = \frac{\epsilon k t}{2} \qquad \text{(A-9)}$$

Introducing the following variables,

$$Z = 8M_\infty A^4\left(\frac{\bar{\chi}_\epsilon^2}{K_\epsilon}\right)^2 \frac{y}{K_\epsilon \chi}\left(\frac{T_\infty}{T_w}\right)^{2(1-\omega)}$$

$$\zeta = 16A^6\left(\frac{\bar{\chi}_\epsilon}{K_\epsilon^{2/3}}\right)^6\left(\frac{T_\infty}{T_w}\right)^{3(1-\omega)} \qquad \text{(A-10)}$$

Eq. (A-9) reduces to

$$Z(ZZ_\zeta)_\zeta - \sqrt{ZZ_\zeta} = 1 \qquad \text{(A-11)}$$

The variables given in Eq. (A-10) reduce to those used by Cheng for the case of $\omega = 1$, and Eq. (A-11) is identical to the governing differential equation solved by Cheng (Eq. (2.17) in Ref. 29). These results show that the arbitrary temperature-viscosity relation can be interpreted rather simply within Cheng's theory if we define a new viscous interaction parameter.

$$\bar{\chi}_\epsilon' = A\sqrt{\frac{C_*'}{C_*}}\left(\frac{T_\infty}{T_w}\right)^{\frac{1-\omega}{2}}\bar{\chi}_\epsilon \qquad \text{(A-12)}$$

Consistent correlations should be obtained by using the new viscous interaction parameter in the existing similarity parameters.

$$\frac{K_\epsilon^2}{(\bar{\chi}_\epsilon')^4}\frac{1}{\gamma}\frac{p}{p_\infty} \text{ and } \epsilon\left(0.664+1.73\frac{T_w}{T_0}\right)A\frac{K_\epsilon^3}{(\bar{\chi}_\epsilon')^6}\frac{1}{\sqrt{\gamma}}M^3C_H \quad \text{vs.} \quad \frac{\bar{\chi}_\epsilon'}{K_\epsilon^{2/3}} \qquad \text{(A-13)}$$

It will be noted that use of the above modified similarity variables requires a knowledge of the constant, A, which in turn requires a solution to the boundary layer equations, Eq. (A-2). Since this constant enters as the fourth and fifth power in these similarity variables it appears that a correlation would be very sensitive to the magnitude of the constant. This sensitivity can be assessed by using an approximate solution. It was shown in Ref. 29 that the pressure distribution on a blunted flat plate is well represented by the sum of the bluntness effects and the displacement effect. The displacement effect, assuming a power law variation for the viscosity, is that given in Ref. 29 with $\bar{\chi}_\epsilon'$ substituted for $\bar{\chi}_\epsilon$. Consequently the surface pressure is

$$\frac{1}{\gamma}\frac{p}{p_\infty} \approx \frac{1}{(18)^{1/3}} K_\epsilon^{2/3}\left[1 + \frac{\sqrt{3}}{2}(18)^{1/3}\frac{\bar{\chi}_\epsilon'}{(K_\epsilon)^{2/3}}\right] \tag{A-14}$$

and the heat transfer is

$$M_\infty^3 C_H = \frac{\phi_{\eta\eta}(0)}{P_r\sqrt{2}}\,\bar{\chi}'\,\frac{p/p_\infty}{\sqrt{\int_0^L \frac{p}{p_\infty}\frac{dx}{L}}} \tag{A-15}$$

where

$$\bar{\chi}' = M_\infty^3\sqrt{\frac{C_*'}{Re_L}}\left(\frac{T_\infty}{T_w}\right)^{\frac{1-\omega}{2}}$$

Substituting the approximate pressure distribution, Eq.(A-14) into Eq. (A-15) yields

$$M_\infty^3 C_H \approx \frac{\phi_{\eta\eta}(0)}{P_r\sqrt{2}}\,\bar{\chi}'\sqrt{\frac{\gamma}{3}}\left(\frac{K_\epsilon}{18}\right)^{1/3}\left[\frac{1 + \frac{\sqrt{3}}{2}(18)^{1/3}\frac{\bar{\chi}_\epsilon'}{(K_\epsilon)^{2/3}}}{\sqrt{1 + \frac{(18)^{1/3}}{\sqrt{3}}\frac{\bar{\chi}_\epsilon'}{(K_\epsilon)^{2/3}}}}\right] \tag{A-16a}$$

Present interests center on dominant bluntness effects, $\bar{\chi}_\epsilon'/(K_\epsilon)^{2/3} < 1$ and Eq. (A-16a) can be simplified to

$$M_\infty^3 C_H \approx \frac{\phi_{\eta\eta}(0)}{P_r\sqrt{2}} \bar{\chi}' \sqrt{\gamma/3} \left(\frac{K_\epsilon}{18}\right)^{1/3} \left[1 + \frac{(18)^{1/3}}{\sqrt{3}} \frac{\bar{\chi}_\epsilon'}{(K_\epsilon)^{2/3}}\right] \tag{A-16b}$$

The effect of power law viscosity relation on the present data can now be assessed from Eq. (A-14) and (A-16b). It can be seen that for small $\bar{\chi}_\epsilon' / (K_\epsilon)^{2/3}$, the surface pressure is essentially unaffected by the exponent in the viscosity relation. However, the heat transfer varies as $\phi_{\eta\eta}(0)\bar{\chi}'$ and consequently is directly influenced by the temperature-viscosity relation. Now, if the pressure and heat transfer, Eq. (A-14) and (A-16b), are cast in terms of the similarity variables,

$$\frac{K_\epsilon^2}{(\bar{\chi}_\epsilon')^4} \frac{1}{\gamma} \frac{p}{p_\infty} \approx \frac{1}{(18)^{1/3}} \left[\frac{(K_\epsilon)^{2/3}}{\bar{\chi}_\epsilon'}\right]^4 \left[1 + \frac{\sqrt{3}}{2} (18)^{1/3} \frac{\bar{\chi}_\epsilon'}{(K_\epsilon)^{2/3}}\right] \tag{A-17}$$

$$\epsilon\,(0.664 + 1.73\ T_w/T_0)\,A \frac{K_\epsilon^3}{(\bar{\chi}_\epsilon')^6} \frac{M_\infty^3 C_H}{\sqrt{\gamma}} \approx \frac{\phi_{\eta\eta}(0)}{P_r\sqrt{6}} \frac{1}{(18)^{1/3}} \left[\frac{(K_\epsilon)^{2/3}}{\bar{\chi}_\epsilon'}\right]^5 \left[1 + \frac{(18)^{1/3}}{\sqrt{3}} \frac{\bar{\chi}_\epsilon'}{(K_\epsilon)^{2/3}}\right] \tag{A-18}$$

it can be seen that for small values of $\bar{\chi}_\epsilon'/(K_\epsilon)^{2/3}$ changes in the viscosity exponent (or changes in $\bar{\chi}_\epsilon'$) cause a change in heat transfer but cause only small change in pressure.

APPENDIX B

MATCHED SIMILARITY BOUNDARY-LAYER SOLUTION

A boundary -layer analysis for flat plate model with a wedge nose is complicated because the boundary layer equations are valid at the wedge shoulder only if the boundary layer thickness is much smaller than the body radius of curvature. This condition is not met in the present experiments, and consequently, a more complicated solution of the Navier-Stokes equations is required in the vicinity of the shoulder. Fortunately, the present purposes do not require a complete solution for the corner flow, but only require that the observed behavior be identified as a boundary layer effect. Consequently, the present requirements are to predict the observed variations in pressure, heat transfer, and displacement thickness with boundary layer theory.

The basis for matched similarity solutions in the present problem can be set out in fairly simple terms. The aim here is to scale the displacement thickness, pressure, and heat transfer observed at some point, station 1, immediately downstream of the wedge shoulder, to those at a station further downstream. The ratio of displacement thickness at any station to that at station 1 is

$$\frac{\delta^*}{\delta_1^*} = \frac{u_\delta}{u_{\delta_1}} \frac{p_1}{p} \sqrt{\frac{\xi}{\xi_1}} \qquad \text{(B-1)}$$

where

$$\xi = \frac{\mu_w}{RT_w} \int_0^L p_w u_\delta \, dx$$

A pressure gradient variable is introduced, $\beta = \frac{1}{p} \frac{dp}{dx}$ and the inviscid momentum equation is used to obtain the identity

$$\beta = \frac{1}{p}\frac{dp}{dx} = -\gamma M_\delta^2 \frac{1}{u_\delta}\frac{du_\delta}{dx} \qquad \text{(B-2)}$$

A third equation is obtained from the Prandtl-Meyer relation for an isentropic flow deflection.

$$\frac{1}{u_\delta}\frac{du_\delta}{dx} = \frac{1}{\sqrt{M_\delta^2 - 1}}\frac{d\psi}{dx} = \frac{1}{\sqrt{M_\delta^2 - 1}}\frac{d^2\delta^*}{dx^2} \qquad \text{(B-3)}$$

Substituting Eq. (B-2) into Eq. (B-3) yields,

$$\beta = -\frac{\gamma M_\delta^2}{\sqrt{M_\delta^2 - 1}}\frac{d^2\delta^*}{dx^2} \approx -\gamma M_\delta \frac{d^2\delta^*}{dx^2} \qquad \text{(B-4)}$$

Differentiating Eq. (B-1) and neglecting terms of order $\frac{1}{M^2}$, $\frac{\delta^*}{M}$, $\beta\delta^*$, yields*,

$$\frac{d\delta^*}{dx} = -\delta^*\beta \qquad \frac{d^2\delta^*}{dx^2} = \delta^*\left[\beta^2 - \frac{d\beta}{dx}\right] \qquad \text{(B-5)}$$

which is substituted into Eq. (B-4) to yield

$$\frac{d\beta}{dx} - \beta^2 - \frac{\beta}{\gamma M_\delta \delta^*} = 0 \qquad \text{(B-6)}$$

It can be shown that the first-order approximation is to neglect the last term in Eq. (B-6). This is tantamount to neglecting velocity variations in calculating the change in displacement thickness. The governing equation is $\frac{d\beta}{dx} - \beta^2 = 0$ with the solution,

$$\beta = \frac{\beta_1}{1 - \beta_1(x - x_1)} \qquad \text{(B-7)}$$

The corresponding values of the displacement thickness, pressure, and heat transfer on the afterbody for the wedge-nose problem are

*It should be noted that in evaluating ξ, the integration is made for the wedge leading edge, and that the wedge pressure is much greater than the afterbody pressure. Consequently terms like $\frac{1}{\xi}\frac{d\xi}{dx}$ are negligible.

$$\frac{\delta^*}{\delta_1^*} \approx 1-\beta_1(x-x_1) \qquad \frac{p}{p_1} \approx \frac{q}{q_1} \approx \frac{1}{1-\beta_1(x-x_1)} \tag{B-8}$$

These are the matched similarity solutions for the flat plate with a wedge nose.

Eq. (B-8) are the matched similarity solutions which provide a basis for investigating the distribution of pressure, heat transfer, and displacement thickness on the afterbody in the present experiments. These first-order solutions do not, however, provide a means for estimating the range of validity for the solutions. This estimate can be obtained from the terms neglected in the formulation. Returning to Eq. (B-6), the complete solution to this equation is

$$\beta = \frac{\beta_1}{1-\beta_1(x-x_1)+\beta_1 f(x)} \tag{B-9a}$$

where

$$f(x) = \int_{x_1}^{x} \frac{dx}{\delta^*\beta\gamma M_\delta} \approx c_1(x-x_1)+c_2(x-x_1)^2$$

$$c_1 = \frac{1}{\gamma M_1\beta_1\delta_1^*} \qquad c_2 = \frac{1}{2\gamma M_1(\beta_1\delta_1^*)^2}\left[\frac{d}{dx}(\beta\delta^*)\right]$$

It follows that the next order of approximation is

$$\beta = \frac{\beta_1}{1-\beta_1(1-c_1)+\beta_1 c_2(x-x_1)^2} \tag{B-9b}$$

Two regions have been excluded from consideration in the foregoing derivation. The first is the immediate neighborhood of the shoulder in which local similarity cannot be expected to apply. Explicitly, this zone is bounded by the conditions

$$\frac{p_1}{p_w} << 1 \qquad \text{and} \qquad \beta\delta^* << 1$$

which correspond to the requirement that $x/t \gtrsim 1.2$ in the present wedge experiments, provided local similarity is valid in this region.

The second excluded zone is the region far removed from the shoulder as embodied in the requirement that

$$\frac{\delta^*}{t} << 1$$

This is not a very stringent condition. Thus the solution as given by Eq. (B-9b) should be expected to hold in a rather large domain.

The solutions as given by Eq. (B-8) will be applicable only over restricted ranges $(x-x_1)$ within this domain. This is a direct consequence of approximations made in the process of integrating Eq. (B-6). Three conditions have been imposed which restrict the range of $(x-x_1)$. Namely,

$$\left| \beta_1 C_2 (x-x_1)^2 \right| << \left| 1 - \beta_1 (1-C_1)(x-x_1) \right| \qquad \text{(a)}$$

$$\left| \tfrac{1}{2} \beta_1^2 C_1 (x-x_1)^2 \right| << \left| 1 - \beta_1 (x-x_1) \right| \qquad \text{(b)}$$

$$\bar{\xi} \sim \bar{\xi}_1 \qquad \text{(c)}$$

The range of validity of Eq. (B-8) is necessarily determined by the most stringent of the conditions listed above. For the wedge experiments, β ranges from about -1 to 0 for $x/t \gtrsim 1.2$. In addition $M \approx 3.5$ and $\delta^*/t \approx 1/6$. Then condition (a) requires that $(x-x_1)$ varies from about 1 to 0.5 as β ranges from -1 to 0. Condition (b) implies that

$(x-x_1)_{max}$ varies from about 0.8 to ∞ over the same range of β. It is easily shown that condition (c) restricts $(x-x_1)_{max}$ to values between about 3 and 4 as β goes from -1 to 0. Consequently, one should expect that solutions given by Eq. (B-8) should begin to deviate significantly from the experimental data at about $x/t \approx 2.1$ if the initial data point $x_1/t \approx 1.3$.

APPENDIX C

THE RESPONSE OF A BOUNDARY LAYER TO A DISCONTINUITY IN SURFACE CURVATURE

A detailed study of this problem would require a solution of the Navier-Stokes equations. Consequently, little reference to it can be found in the theoretical literature. However, it is possible to determine some aspects of the gross behavior of the boundary layer by using an integral approach and examining the behavior of the rate of growth of the displacement thickness immediately to the right and left of a discontinuity in surface curvature. This approach was first used by Stroud[35]. In the following, Stroud's approach will be generalized in an attempt to explain some of the flowfield phenomena which have been observed in the experiments reported here.

The momentum integral equation for compressible flow is[33, 35]

$$\frac{d\theta}{ds} = \frac{C_f}{2} - \frac{\theta}{\rho_e}\frac{d\rho_e}{ds} - (2+H)\frac{\theta}{u_e}\frac{du_e}{ds} \tag{C-1}$$

where S is the surface coordinate. C_f is the skin friction coefficient, θ is the momentum thickness, the subscript e refers to condition along the edge of the boundary layer, and H is the form factor defined as

$$H = \delta^*/\theta \tag{C-2}$$

where δ^* is the displacement thickness. It can be shown that

$$H \simeq \frac{\gamma-1}{2} M_e^2 \tag{C-3}$$

in the cold wall limit. The terms involving the edge conditions can be combined so that Eq. (C-1) can be written in the form:

$$\frac{d\theta}{ds} = \frac{C_f}{2} + \left(\frac{3-\gamma}{2} M_e^2 - 2\right)\frac{\theta}{u_e}\frac{du_e}{ds} \qquad \text{(C-4)}$$

Now the Prandtl-Meyer relation is

$$\frac{1}{u_e}\frac{du_e}{ds} = -\frac{1}{\sqrt{M_e^2-1}}\frac{d\alpha}{ds}$$

where α is the local inviscid flow angle. Now

$$\tan\alpha = \frac{d_{\delta^*}}{ds} + \frac{dy_b}{ds}$$

where y_b is the body coordinate. It follows that

$$\frac{d\alpha}{ds} = \frac{\frac{1}{R_{\delta^*}} + \frac{1}{R_b}}{1+\left(\frac{1}{R_{\delta^*}}+\frac{1}{R_b}\right)^2}$$

where R_b and R_{δ^*} are the radius of curvature of the body and the boundary layer, respectively. Therefore, Eqs. (C-4) can be written in the form

$$\frac{d_{\delta^*}}{ds} = \left(\frac{\gamma-1}{4}\right) M_e^2 C_f + \frac{2\delta^*}{M_e} - \left(\frac{3-\gamma}{2} M^2 - 2\right)\frac{\delta^*}{\sqrt{M_e^2-1}}\left[\frac{\frac{1}{R_{\delta^*}}+\frac{1}{R_b}}{1+\left(\frac{1}{R_{\delta^*}}+\frac{1}{R_b}\right)^2}\right] \qquad \text{(C-5)}$$

Now we are in a position to draw several interesting conclusions. First of all, the effect of surface curvature appears only in the last term whose magnitude must be comparable to that of the two leading terms if curvature effects are to be important. The last term is very small in the flat plate limit, and vanishes identically when

$$M_e = \sqrt{4/(3-\gamma)} \tag{C-6}$$

which is about 1.58 for a γ of 1.4.

First, consider the case shown in Fig. 13a where a cylinder of radius, R_N, is joined to a flat plate. The flow will always be directed from the left to the right in these examples. Therefore the problem considered here is pertinent to the cylindrically blunted flat plate. Immediately to the left of the cylinder-plate junction,

$$\left(\frac{d\delta^*}{ds}\right)_L = \left\{\frac{\gamma-1}{4} M_e C_f + \frac{2\delta^*}{M} - \left(\frac{3-\gamma}{2} M^2 - 2\right)\frac{\delta^*}{\sqrt{M_e^2-1}}\left[\frac{\frac{1}{R_{\delta^*}} + \frac{1}{R_N}}{1+\left(\frac{1}{R_{\delta^*}}+\frac{1}{R_M}\right)^2}\right]\right\}_L$$

while immediately to the right,

$$\left(\frac{d\delta^*}{ds}\right)_R = \left\{\frac{\gamma-1}{4} M_e^2 C_f + \frac{2\delta^*}{M_e} - \left(\frac{3-\gamma}{2} M_e^2 - 2\right)\frac{\delta^*}{\beta}\left[\frac{\frac{1}{R_{\delta^*}}}{1+\frac{1}{R_{\delta^*}^2}}\right]\right\}_R$$

On physical grounds, one would expect that C_f, δ^*, and $d\delta^*/ds$ would be continuous. If $d\delta^*/ds$ is continuous then M_e must be also. Therefore, it is necessary that

$$\frac{1}{R_{\delta^*_R}} = \frac{1}{R_{\delta^*_L}} + \frac{1}{R_N}$$

In most cases of interest, the boundary layer is thin so that

$$R_{\delta^*_R} \simeq \frac{R_N}{2}$$

Thus a discontinuity in surface curvature generates a discontinuity in boundary layer curvature. Moreover, the effect tends to produce an over-expansion at the discontinuity which must result in a recompression. This is consistent with Schlieren photographs of this type of flow in which a weak shock was found which appeared to originate at the cylinder-plate junction. Although this result was obtained for a thin boundary layer, it is not difficult to see that the effect increases with boundary layer thickness.

In the case where the flow about the cylinder is compressive, as in Fig. 13b, the flow over-compresses but a shock is formed in this case anyway.

Now consider the flow about the same sort of body but with the geometry reversed with respect to the flow direction as in Fig. 13c. Then it follows immediately that

$$\frac{1}{R_{\delta^*_L}} = \frac{1}{R_{\delta^*_R}} + \frac{1}{R_N}$$

which implies that

$$R_{\delta^*_R} \simeq -R_N$$

when the plate boundary layer is thin. Thus we are led to the result that a compressive flow is generated at a convex surface. This effect is reduced as the boundary layer thickness increases.

When the corner is compressive, the flow tends to expand at first as shown in Fig. 13d. This behavior is qualitatively verified by Holden's schlieren data[43] obtained with a flapped flat plate. These data suggest the flow initially expands as indicated in Fig. 13d. A shock will form in this case anyway and the boundary layer would not be expected to change the appearance of the flowfield.

Of particular interest in connection with the experiments reported here is the behavior of the boundary layer at a corner. The corner geometry can be regarded as a combination of two cases already discussed, Fig. 13c and 13a. Assuming that the boundary layer is initially thin, we can immediately write the result for the upstream surface curvature discontinuity, Fig. 13c, which is

$$R_{\delta^*_{RU}} \simeq -R_c$$

where R_c is the corner radius. For the downstream discontinuity, the previously derived results for Fig. 13a indicate that

$$\frac{1}{R_{\delta^*_{RD}}} = \frac{1}{R_{\delta^*_{LD}}} + \frac{1}{R_C}$$

Although $R_{\delta^*_{LD}}$ is not known, one might suspect that the second term dominates when the corner is sufficiently sharp, i.e.,

$$R_{\delta^*_{RD}} \simeq R_C$$

When the corner radius is sufficiently large no discontinuity in curvature appears, as one would expect. Therefore, it appears that a locally compressive flow generated by boundary layer thickening should appear on a convex corner which is sufficiently sharp. The qualitative boundary layer behavior is sketched in Fig. 13e. The similarity between this sketch and the Schlieren photograph shown in Fig. 8 strongly suggests that the mechanism described here is responsible for the corner shock.

REFERENCES

1. Lick, W., Inviscid Flow Around a Blunt Body of a Reacting Mixture of Gases. Renssalaer Polytech. Inst. TR AE 5810 (May 1958) and TR AE 5814 (December 1958).
2. Freeman, N. C., Dynamics of a Dissociating Gas: III. Nonequilibrium Theory. J. Fluid Mech. 4, 4 (1958).
3. Gibson, W. E., Dissociation Scaling for Nonequilibrium Blunt-Nose Flows. AEDC-TDR-62-25, CAL Rept. AF-1560-A-1 (February 1962); Also ARS Journal 32, 2 (February 1962).
4. Hall, J. G., Eschenroeder, A. Q., and Marrone, P. V., Blunt-Nose Inviscid Airflows with Coupled Nonequilibrium Processes. J. Aerospace Sci. 29, 9, 1038-1051 (September 1962).
5. Wood, A. D., Springfield, J. F., and Pallone, A. J., Chemical and Vibrational Relaxation of an Inviscid Hypersonic Flow. AIAA J. 2, 10 (1964).
6. Ivey, H. R. and Cline, C. W., Effect of Heat-Capacity Lag on the Flow Through Oblique Shock Waves. NACA TN 2196 (October 1950).
7. Bethe, H. A. and Teller, E., Deviations from Thermal Equilibrium in Shock Waves. Aberdeen Proving Ground, BRL Rept. X-117 (1945).
8. Moore, F. K. and Gibson, W. E., Propagation of Weak Disturbances in a Gas Subject to Relaxation Effects. IAS Preprint No. 59-64 (January 1959); Also J. Aero/Space Sci. 27, 2 (February 1960).
9. Dressler, F. R., Shock Profiles in Hypersonic Flow of a Relaxing Gas About a Wedge. Cornell Univ. Rept. (no no.) (1961).
10. Sedney, R., South, J. C., and Gerber, N., Characteristic Calculation of Nonequilibrium Flows. Aberdeen Proving Ground, BRL Rept. 1173 (April 1962).

11. Vincenti, W. G., Linearized Flow Over a Wedge in a Nonequilibrium Oncoming Stream. Stanford Univ. Rept. SUDAER 123 (1962).

12. Capiaux, R. and Washington, M., Nonequilibrium Flow Past a Wedge. AIAA J. 1, 3 (1963).

13. South, J. C., Application of the Method of Integral Relations to Supersonic Nonequilibrium Flow Past Wedges and Cones. NASA TR R-205 (August 1964).

14. Lee, R. S., A Unified Analysis of Supersonic Nonequilibrium Flow Over a Wedge: I. Vibrational Nonequilibrium. AIAA J. 2, 4 (1964).

15. Wood, W. W. and Parker, F. R., Structure of a Centered Rarefaction Wave in a Relaxing Gas. Phys. Fluids 1, 3 (1958).

16. Napolitano, L. G., Nonequilibrium Centered Rarefaction for a Relaxing Mixture. AEDC-TN-60-129 (June 1960).

17. Bloom, M. H. and Steiger, M. H., Inviscid Flow with Nonequilibrium Molecular Dissociation for Pressure Distributions Encountered in Hypersonic Flight. J. Aero. Sci. 27, 11 (1960).

18. Appleton, J. P., The Structure of a Prandtl-Meyer Expansion Fan in an Ideal Dissociating Gas. Univ. of Southampton Rept. 146 (August 1960).

19. Glass, I. I. and Kawada, H., Prandtl-Meyer Flow of Dissociated and Ionized Gases. Univ. of Toronto, UTIA Rept. 85 (1962).

20. Glass, I. I. and Takano, A., Nonequilibrium Expansion Flow of Dissociated Oxygen Around a Corner. Univ. of Toronto, UTIA Rept. 91 (1963).

21. Arave, R. J., Centered Rarefaction Wave in a Chemically Reacting Gas. Boeing Rept. D2-22534 (1963).

22. Hall, J. G. and Hertzberg, A., Recent Advances in Transient Surface Temperature Thermometry. Jet Propulsion 28, 11 (November 1958).

23. Vidal, R. J., Model Instrumentation Techniques for Heat Transfer and Force Measurements in a Hypersonic Shock Tunnel. CAL Rept. AD-917-A-1, WADC TN 56-315, AD 97038 (February 1956).

24. Skinner, G. T., Calibration of Thin-Film Gauge Backing Materials. ARS Journal 31, 5, 671-672 (May 1961).

25. Martin, J. F., Duryea, G. R., and Stevenson, L. M., Instrumentation for Force and Pressure Measurements in a Hypersonic Shock Tunnel. Proceedings of the Second Symposium on Hypervelocity Techniques, Univ. of Denver, Denver, Colo., 20-21 March 1962. Arthur M. Krill (Ed.), Plenum Press, New York, 1962.

26. Anonymous, Experimental Facilities Division Hypersonic Shock Tunnel, Description and Capabilities. CAL Rept. (October 1964).

27. Hilton, J., Fabian, G. J., Golian, T. C., Wilson, M. R., and Somers, L., Development and Performance of the CAL Six-Foot Shock Tunnel. CAL Rept. (to be published).

28. Eschenroeder, A. Q., Boyer, D. W., and Hall, J. G., Nonequilibrium Expansions of Air with Coupled Chemical Reactions. Phys. Fluids 5, 615 (1962).

29. Cheng, H. K., Hall, J. G., Golian, T. C., and Hertzberg, A., Boundary-Layer Displacement and Leading-Edge Bluntness Effects in High-Temperature Hypersonic Flow. J. Aero/Space Sci. 28, 5 (May 1961).

30. Hall, J. G. and Golian, T. C., Shock-Tunnel Studies of Hypersonic, Flat-Plate Airflows. CAL Rept. AD-1052-A-10 (December 1960).

31. Blackman, V. H., Vibrational Relaxation in Oxygen and Nitrogen. J. Fluid Mech. 1, 61 (1956).

32. Hall, J. G., Effects of Ambient Nonuniformities in Flow over Hypersonic Test Bodies. CAL Rept. 128 (August 1963).

33. Hunt, B. L. and Sibulkin, M., An Estimate of Compressible Boundary Layer Development Around a Convex Corner in Supersonic Flow. Div. of Engineering, Brown Univ. Rept. (no no.) (November 1964).

34. Weinbaum, S., The Rapid Expansion of a Supersonic Shear Flow. AVCO Res. Rept. 204 (January 1965).

35. Stroud, J., Effect of a Discontinuity in Wall Curvature on the Boundary Layer. ARS Journal, 664-665 (May 1961).

36. Marrone, P. V., Inviscid, Nonequilibrium Flow Behind Bow and Normal Shock Waves, Part I. General Analysis and Numerical Examples. CAL Rept. QM-1626-A-12(I) (May 1963).

37. Garr, L. J. and Marrone, P. V., Inviscid, Nonequilibrium Flow Behind Bow and Normal Shock Waves, Part II. The IBM Computer Programs. CAL Rept. QM-1626-A-12(II) (May 1963).

38. Wray, K. L., A Shock Tube Study of the Vibrational Relaxation of Nitric Oxide. AVCO Res. Rept. 96 (June 1961).

39. Treanor, C. E. and Marrone, P. V., Effect of Dissociation on the Rate of Vibrational Relaxation. Phys. Fluids 5, 9, 1022-1026 (September 1962).

40. Bauer, S. H. and Tsang, S. C., Mechanism for Vibrational Relaxation at High Temperatures. Phys. Fluids 6, 2, 182-189 (February 1963).

41. Hurle, I. R., Russo, A. L., and Hall, J. G., Experimental Studies of Vibrational and Dissociative Nonequilibrium. J. Chem. Phys. 40, 2076 (1964).

42. Vidal, R. J., High Temperature Phenomena in Hypersonic Flows, Final Report. CAL Rept. AF-1560-A-6, AEDC-TDR-64-143 (June 1964).

43. Holden, M., Separated Flow Studies at Hypersonic Speeds, Part II. Two-Dimensional Wedge Separated Flow Studies. CAL Rept. AF-1285-A-13(2) (December 1964).

44. Wagner, Richard D. and Watson, Ralph, Reynolds Number Effects on the Induced Pressure of Cylindrical Bodies with Different Nose Shapes and Nose Drag Coefficients in Helium at a Mach Number of 24. NASA TR R-182 (November 1963).

TABLE I SUMMARY OF TEST CONDITIONS

Test Identification	Facility	Reservoir Conditions Temperature °K	Reservoir Conditions Pressure psia	Ambient Conditions at the Model Station Density Ratio ρ/ρ_{SL}	Ambient Conditions at the Model Station Velocity Ft/Sec	Ambient Conditions at the Model Station Mach Number	Ambient Conditions at the Model Station Reynolds Number/in
Large Scale Model							
High Temp. No. 1	6-ft. Shock Tunnel	6650	16,700	2.28×10^{-4}	14,900	16.3	2680
High Temp. No. 2	6-ft. Shock Tunnel	6200	9,900	5.50×10^{-4}	14,580	12.0	3940
High Temp. No. 3	6-ft. Shock Tunnel	6250	11,050	2.47×10^{-4}	14,750	14.3	2320
Low Temperature	4-ft. Shock Tunnel	3290	3,820	6.01×10^{-4}	9,370	15.0	9210
Small Scale Model							
High Temperature	6-ft. Shock Tunnel	6570	15,620	5.26×10^{-5}	14,800	22.4	1082
Low Temperature	4-ft. Shock Tunnel	3180	750	5.75×10^{-5}	9,210	17.5	1216

TABLE II SUMMARY OF GAS COMPOSITION FOR

CONDITIONS OF FIRST HIGH TEMPERATURE TEST

LOCATION	$X_{O_2}^{*}$	X_{N_2}	X_{NO}	X_O	X_A	X_N
Freestream**	.161	.736	.0692	.0241	9.23×10^{-3}	10^{-13}
Wedge Shoulder**	.1248	.711	.0731	.0809	8.94×10^{-3}	6.03×10^{-4}

* X_i mole fraction of species i

** Vibrational equilibrium is assumed

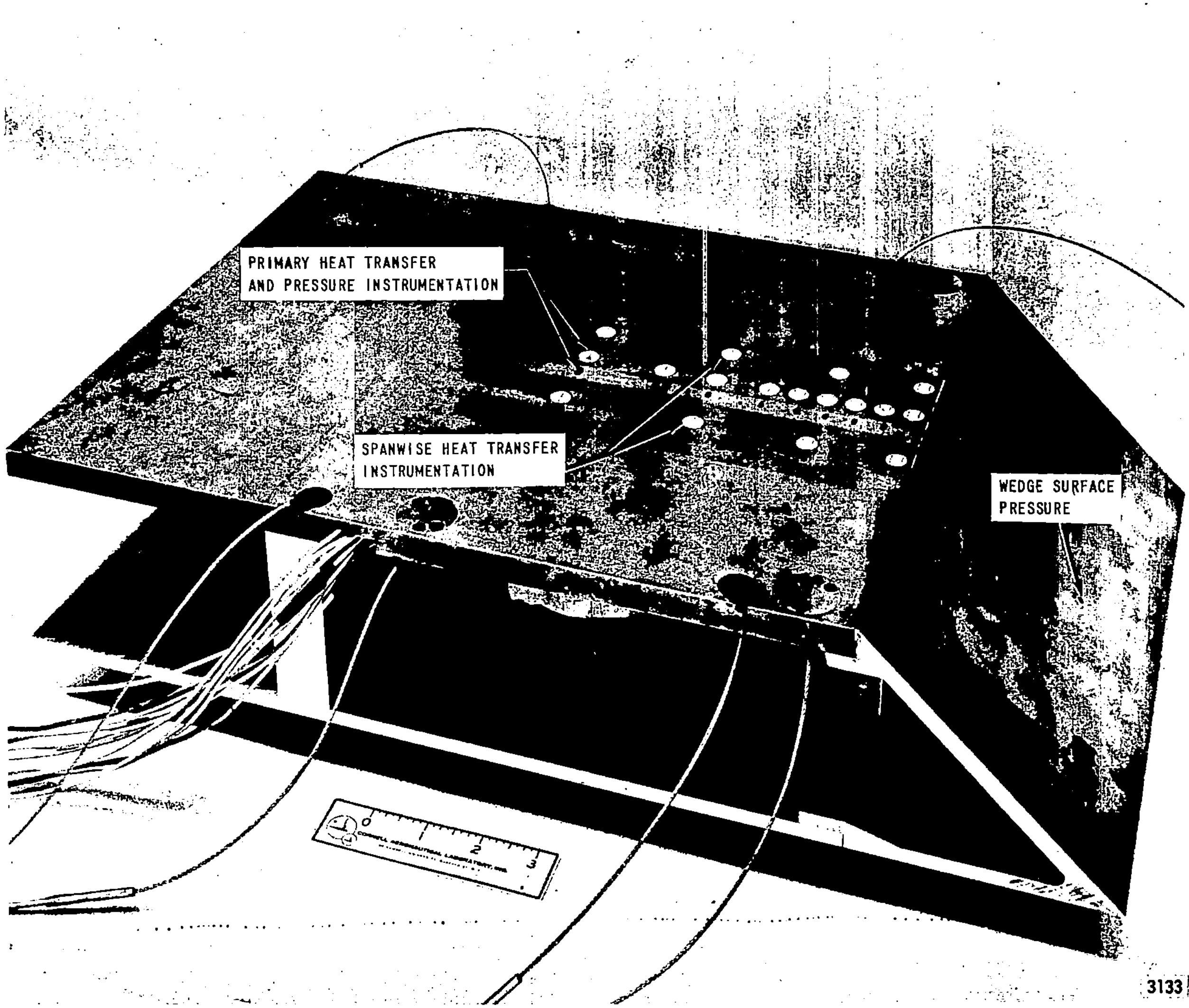

Figure 1 FLAT PLATE MODEL WITH WEDGE LEADING EDGE

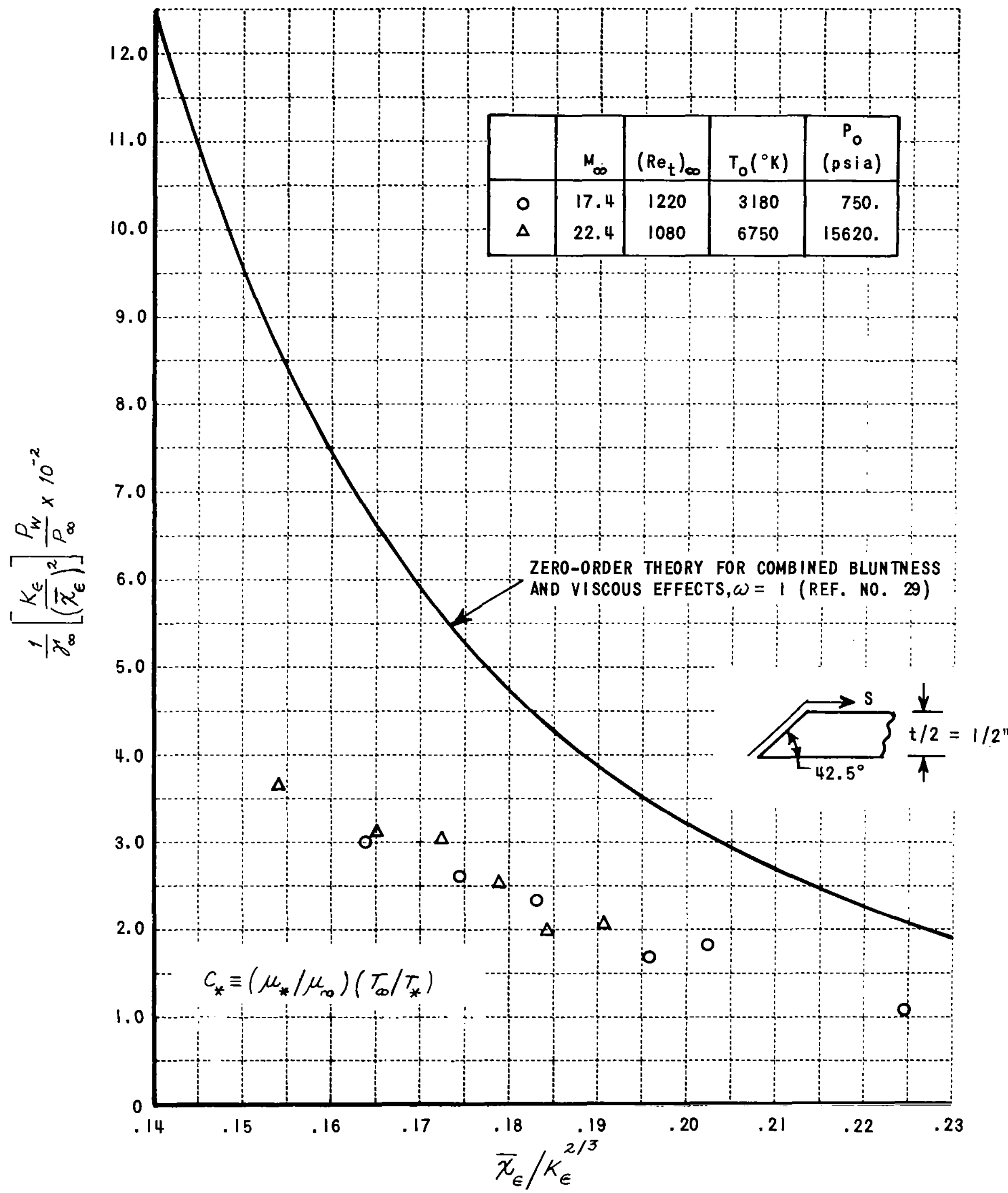

Figure 2 COMPARISON OF IDEAL-GAS THEORY AND EXPERIMENT FOR SURFACE PRESSURE (ASSUMING $\mu \propto T$)

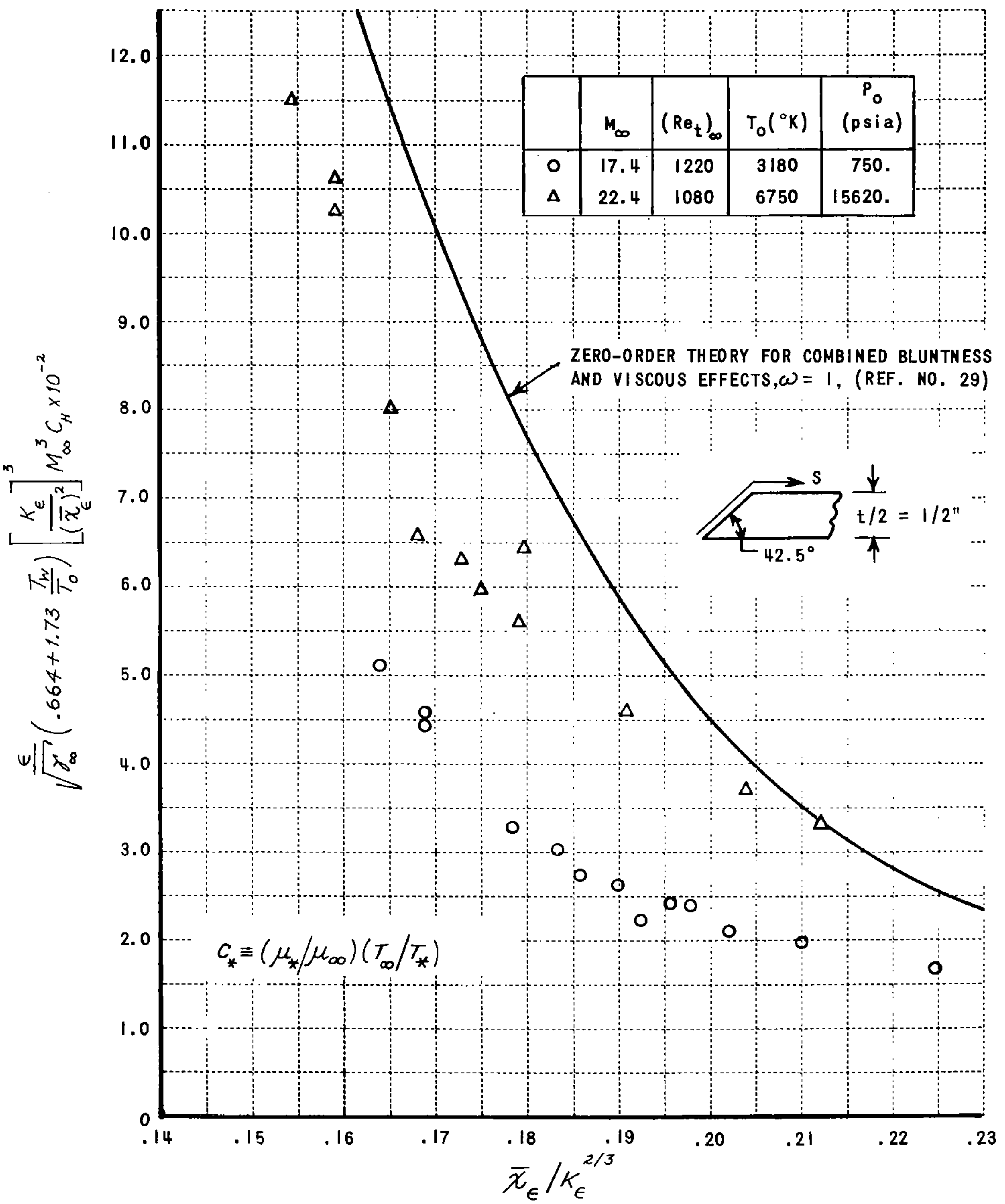

Figure 3 COMPARISON OF IDEAL-GAS THEORY AND EXPERIMENT FOR HEAT TRANSFER (ASSUMING $\mu \propto T$)

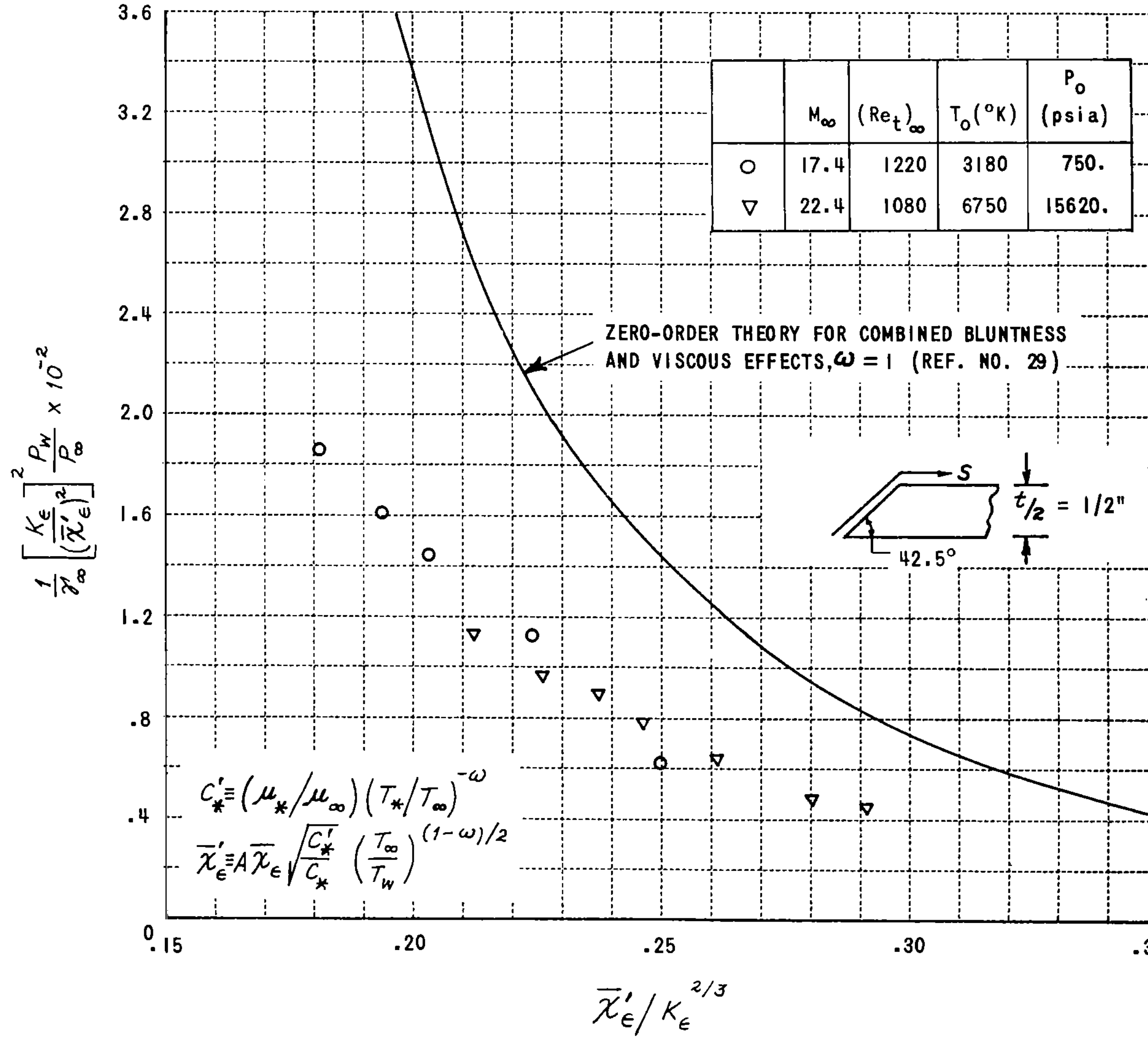

Figure 4 COMPARISON OF MODIFIED THEORY AND EXPERIMENT FOR SURFACE PRESSURE (ASSUMING $\mu \propto T^\omega$)

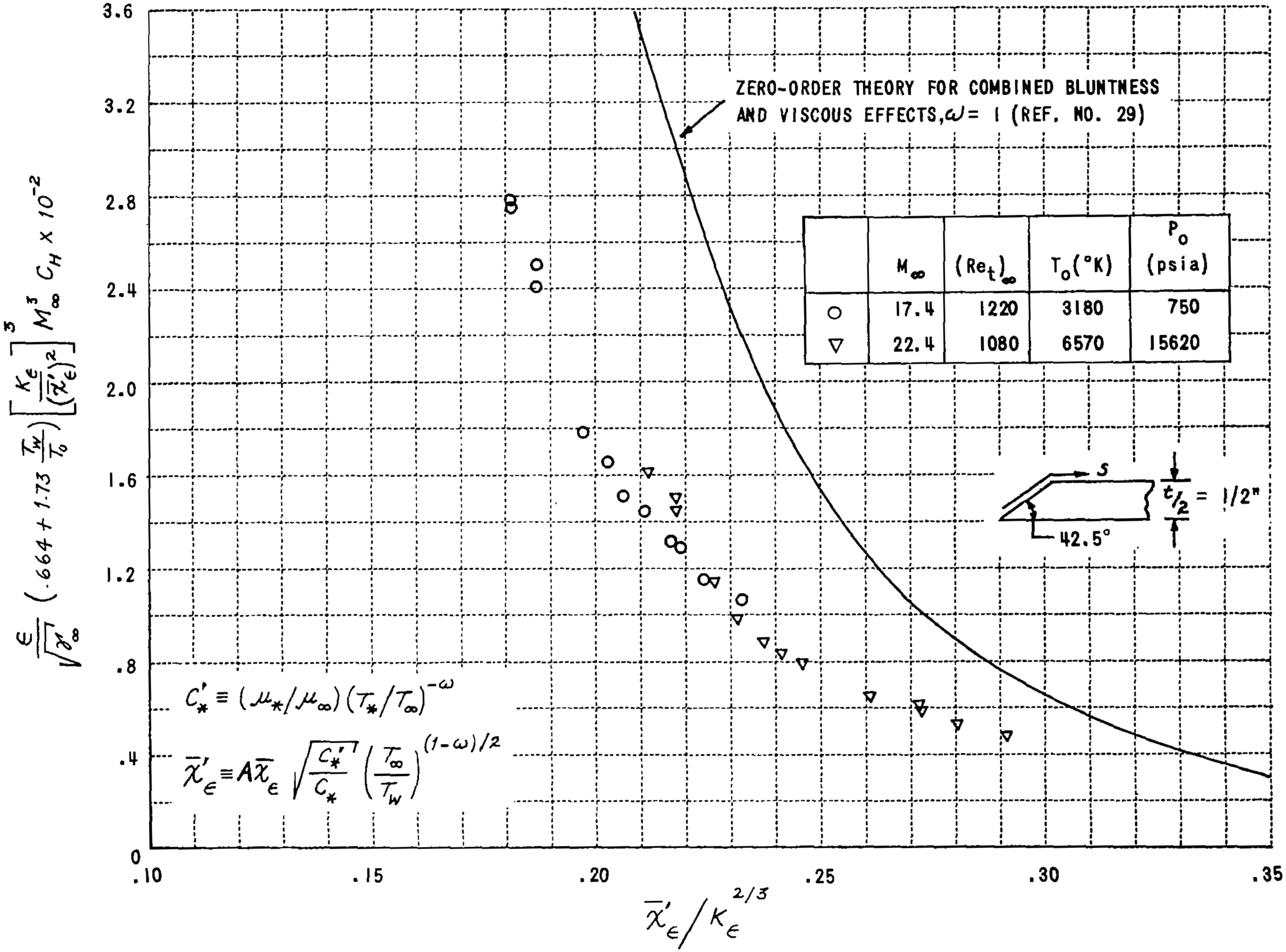

Figure 5 COMPARISON OF MODIFIED THEORY AND EXPERIMENT FOR HEAT TRANSFER
(ASSUMING $\mu \propto T^{\omega}$)

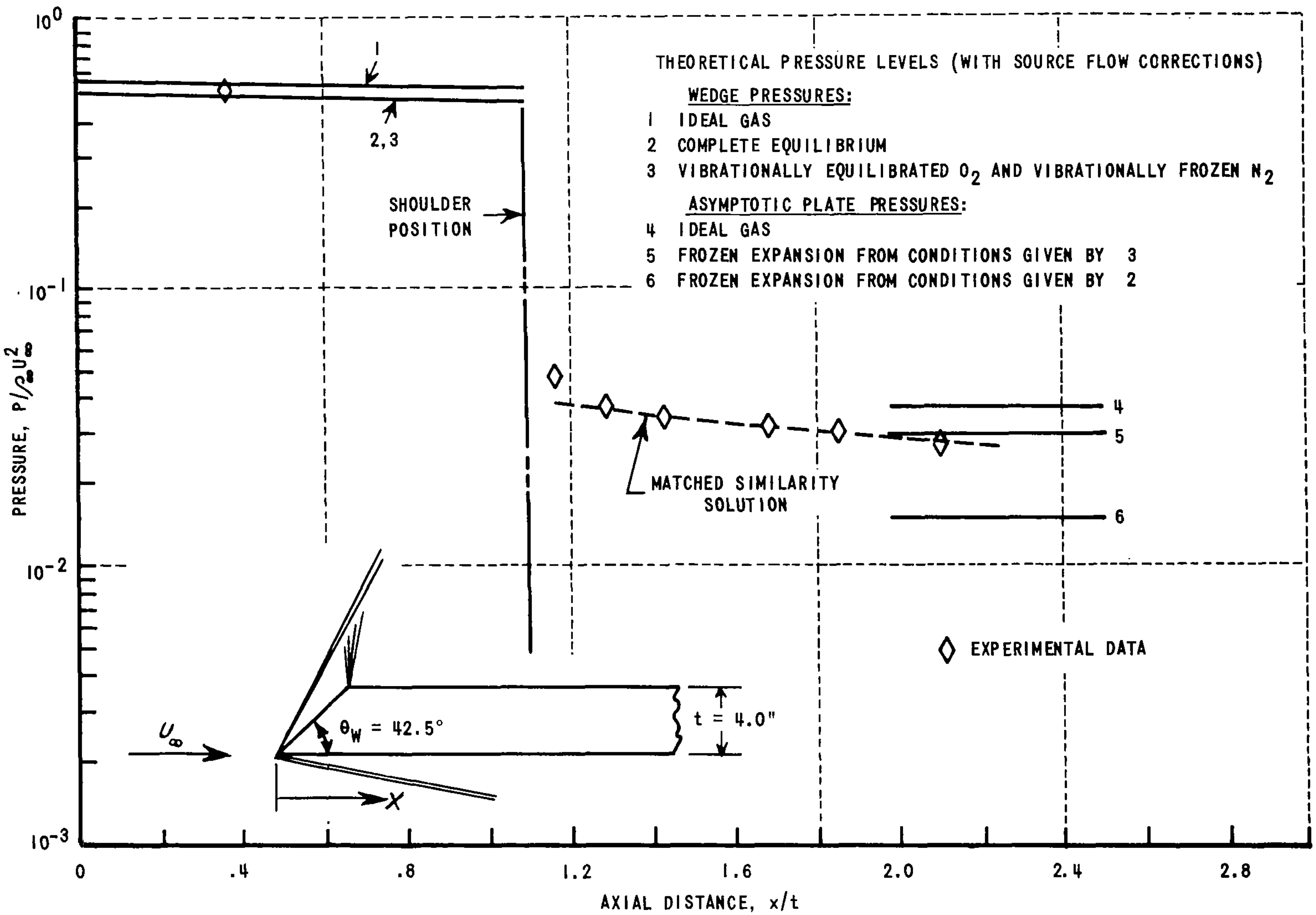

Figure 6 PRESSURE DISTRIBUTION ON A WEDGE-NOSED FLAT PLATE

LOW TEMPERATURE RUN

T_o = 3290°K M_∞ = 15.0 Re_∞/IN = 9210 U_∞ = 9370 FT/SEC

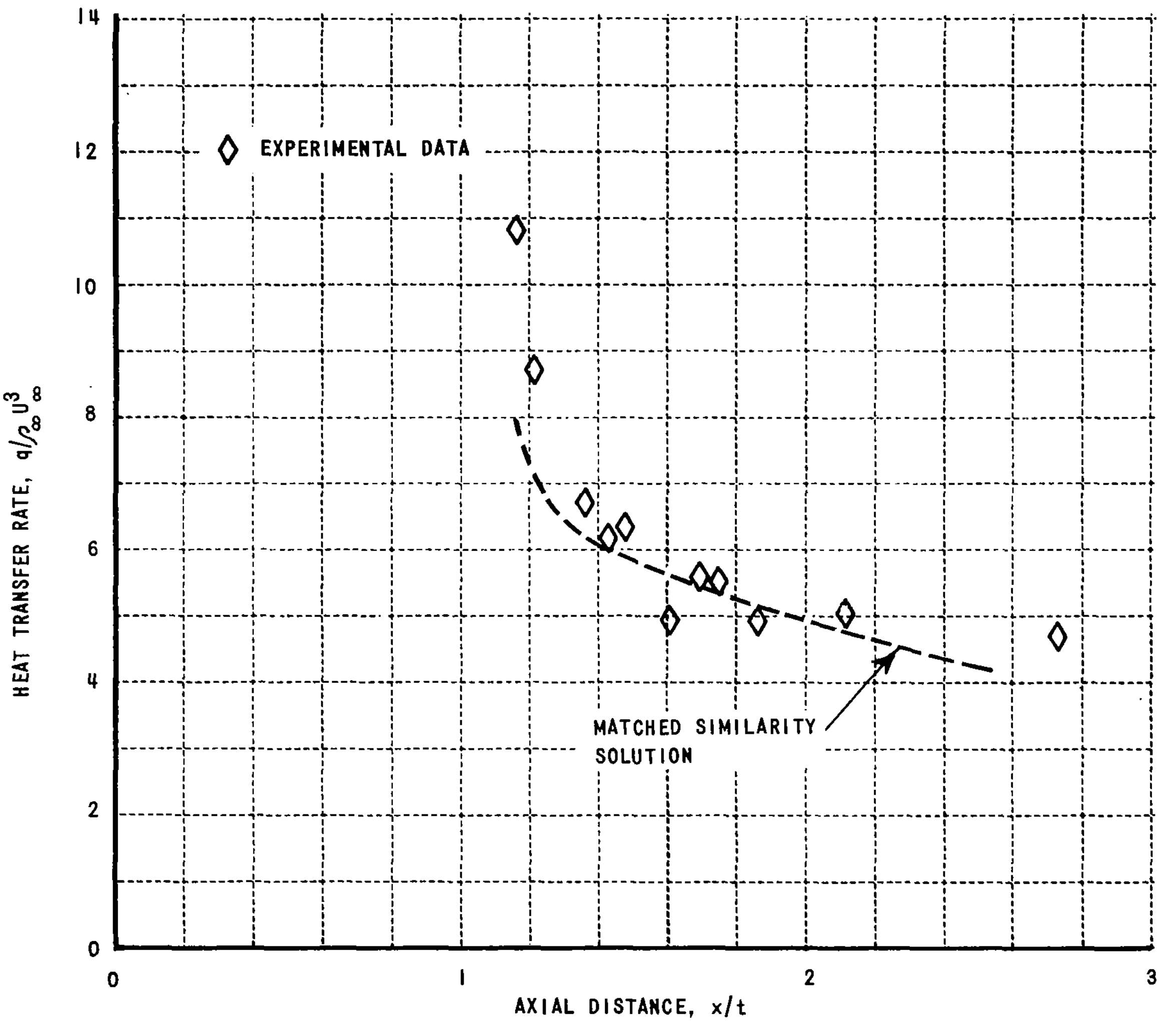

Figure 7 HEAT TRANSFER DISTRIBUTION
LOW TEMPERATURE TEST
T_o = 3290°K M_∞ = 15.0
Re_∞/IN = 9210 U_∞ = 9370 FT/SEC

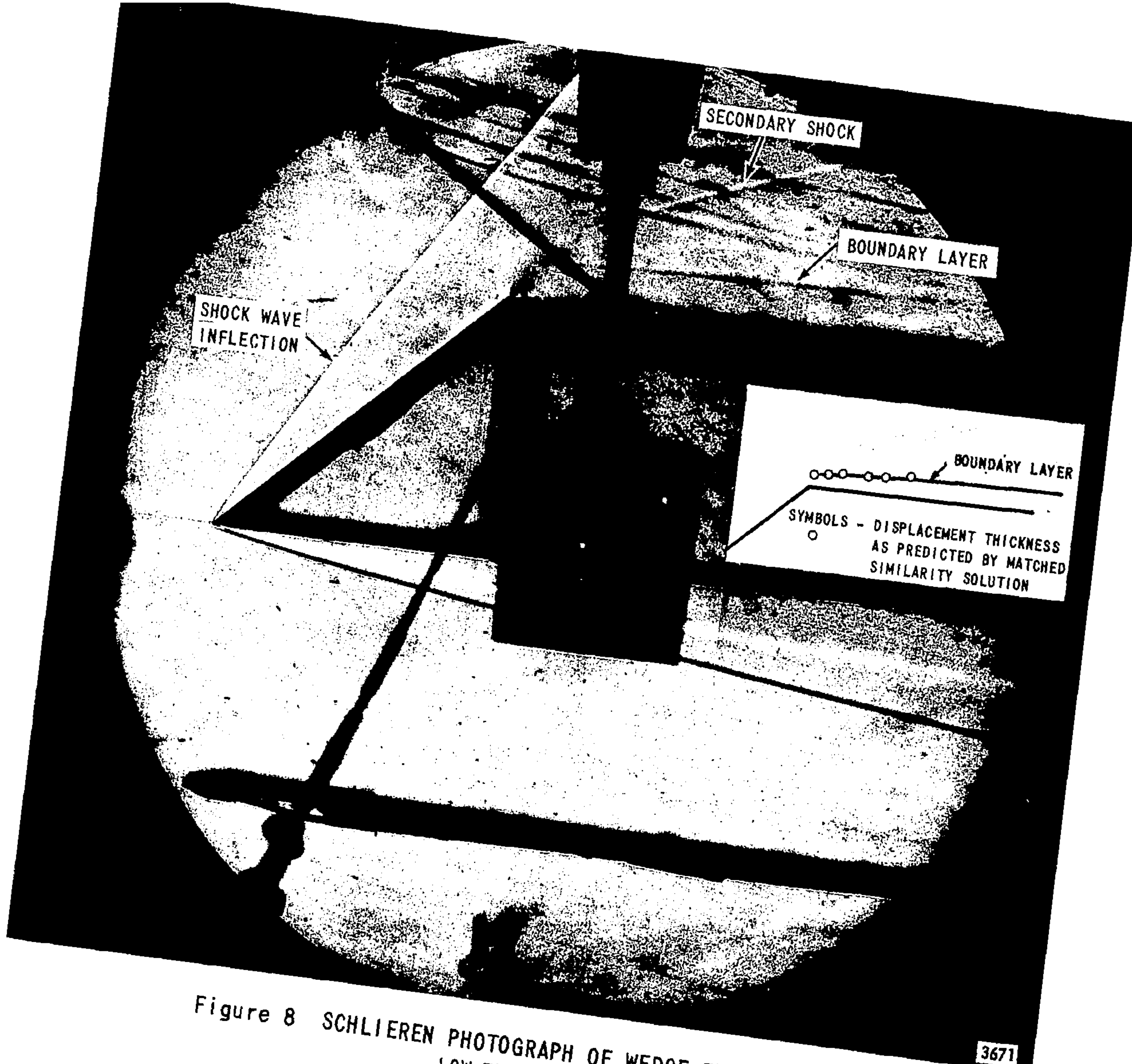

Figure 8 SCHLIEREN PHOTOGRAPH OF WEDGE FLOW FIELD
LOW TEMPERATURE EXPERIMENT
$M_\infty = 15.0 \quad Re_\infty = 9210\ /IN$
$T_o = 3290\ °K \quad U_\infty = 9370$ f.p.s.

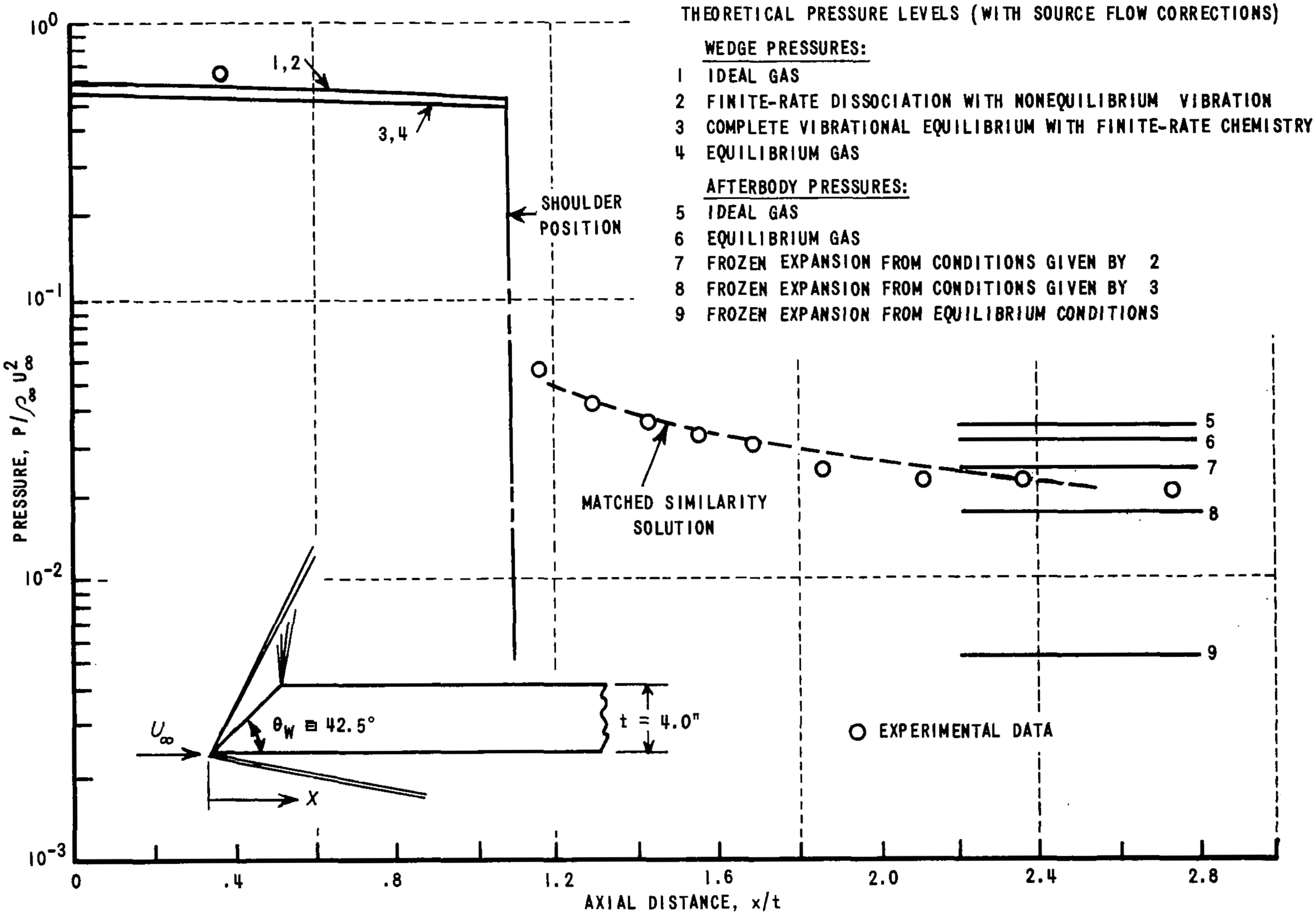

Figure 9 PRESSURE DISTRIBUTION ON A WEDGE-NOSED FLAT PLATE

HIGH TEMPERATURE TEST NUMBER 1

$T_o = 6650°K$ $M_\infty = 16.3$ $Re_\infty/IN = 2680$ $U_\infty = 14,900$ FT/SEC

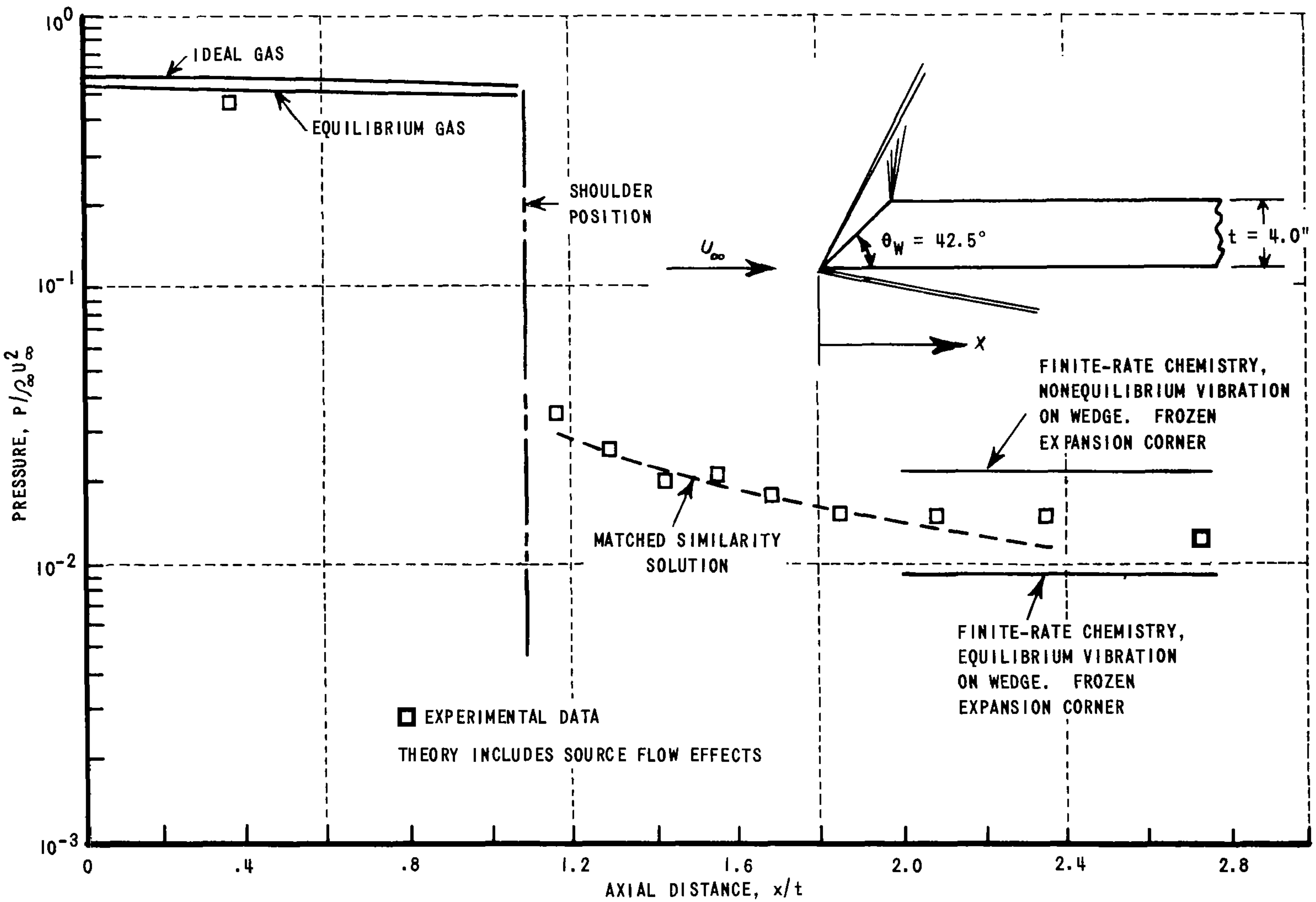

Figure 10 PRESSURE DISTRIBUTION ON A WEDGE-NOSED FLAT PLATE

HIGH TEMPERATURE TEST NUMBER 2

T_o = 6200°K M_∞ = 12.0 Re_∞/IN = 3940 U_∞ = 14,580 FT/SEC

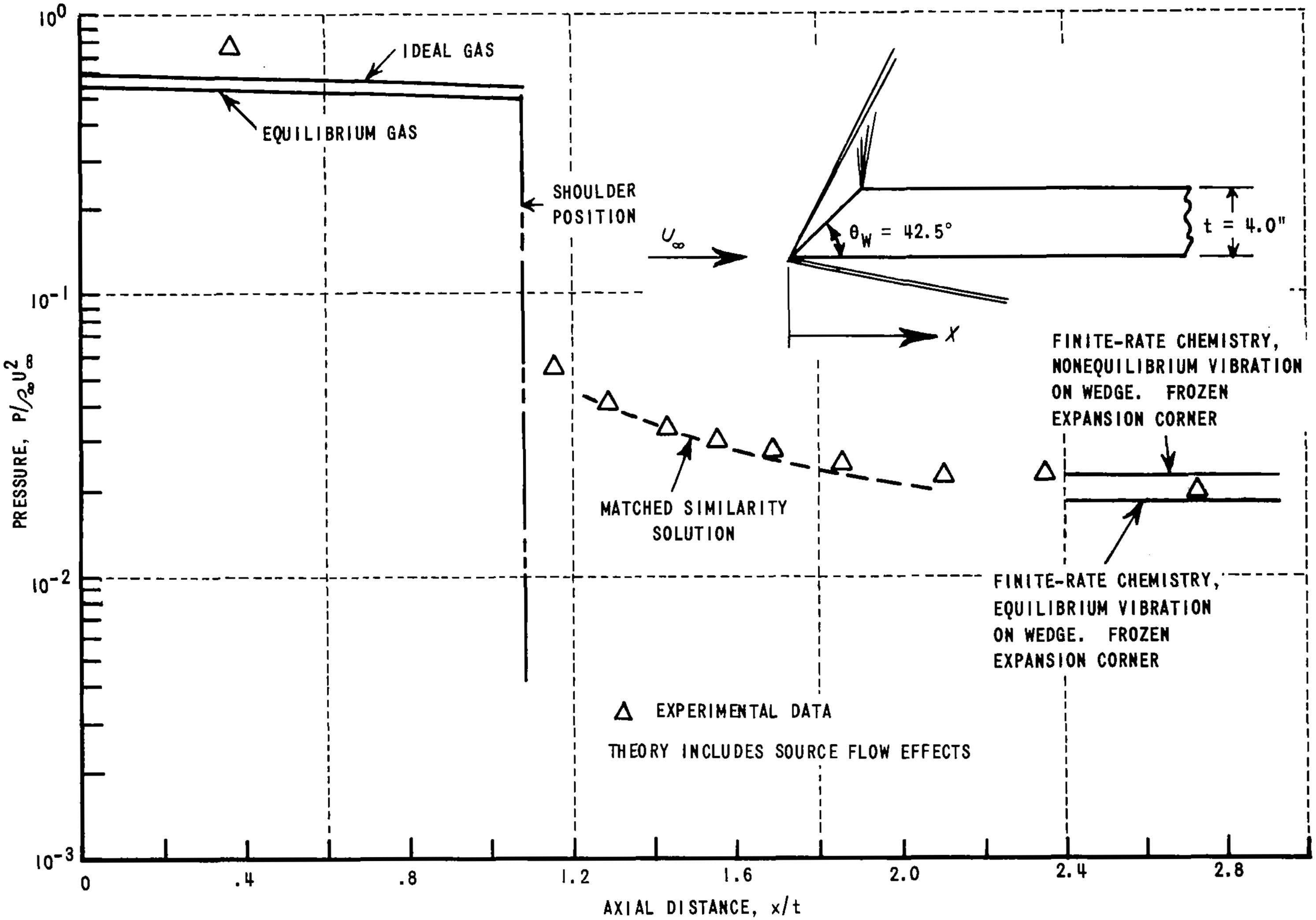

Figure 11 PRESSURE DISTRIBUTION ON A WEDGE-NOSED FLAT PLATE

HIGH TEMPERATURE TEST NUMBER 3

T_o = 6250°K M_∞ = 14.25 Re_∞ /IN = 2320 U_∞ = 14,750 FT/SEC

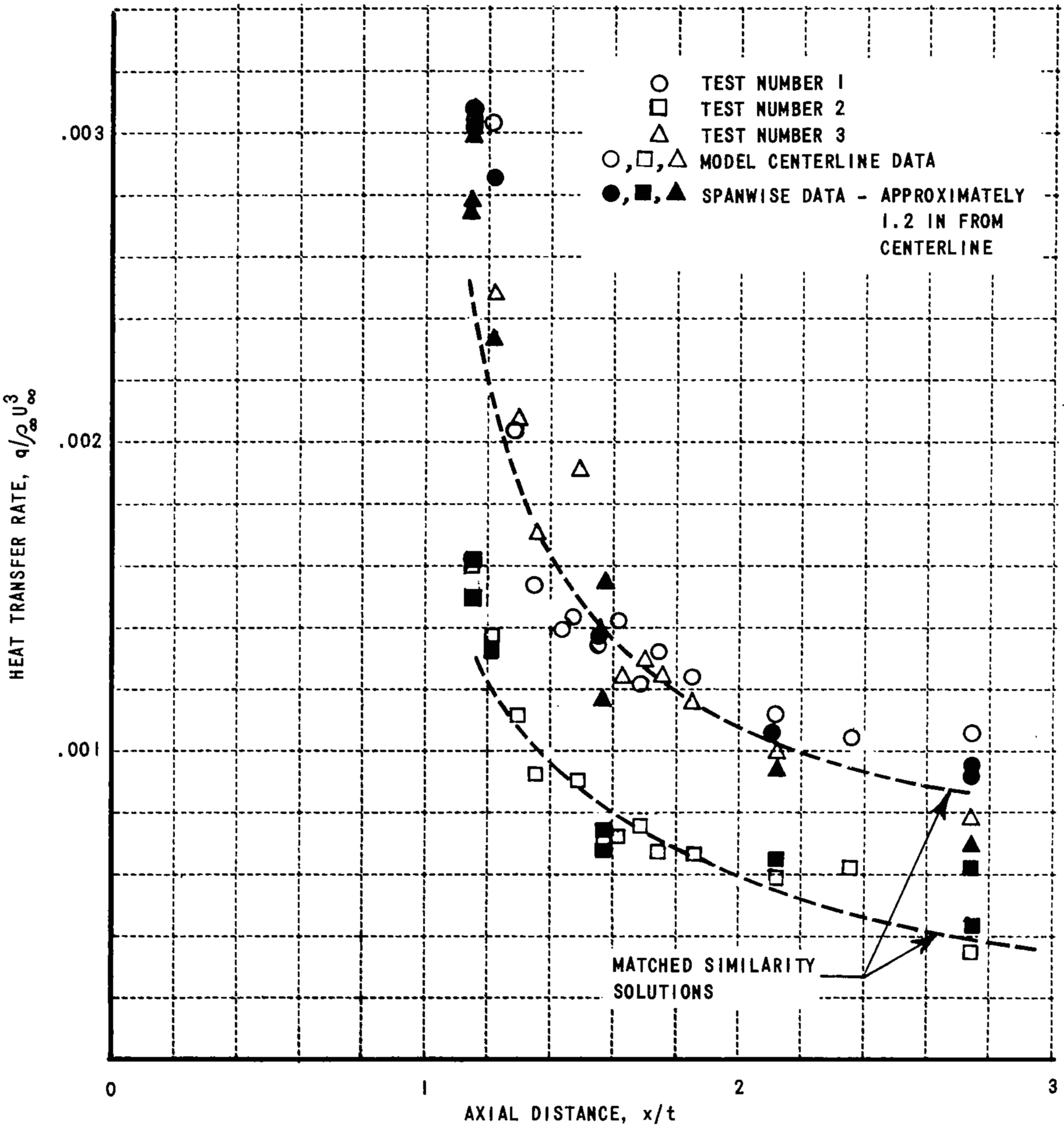

Figure 12 HEAT TRANSFER DISTRIBUTION
HIGH TEMPERATURE TESTS

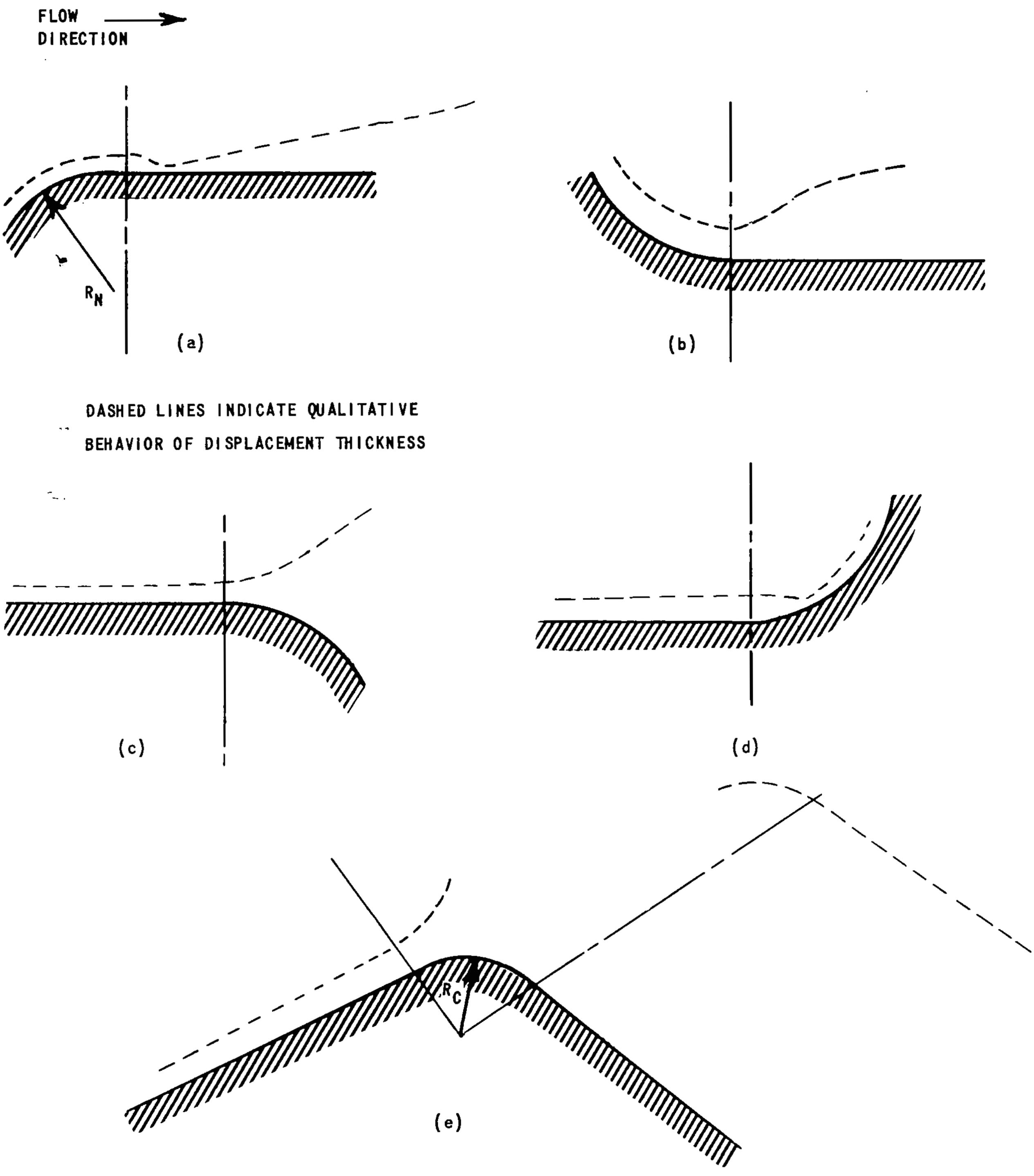

Figure 13 THE RESPONSE OF THE BOUNDARY LAYER TO A DISCONTINUITY IN SURFACE CURVATURE